ENERGY EFFICIENCY AND EMISSION IMPACTS OF HYBRID ENERGY SYSTEMS FOR PUBLIC BUILDINGS: ANALYZING THE ROLE OF BOILERS, NATURAL GAS, AND GASOLINE GENERATORS

Aykut Fatih GÜVEN[1]

[1]Yalova University, Faculty of Engineering, Department of Electrical and Electronics Engineering, Yalova-Türkiye
[1]ORCID: https://orcid.org/0000-0002-1071-9700

Necat UZUNER[2]

[2]Yalova University, Faculty of Engineering, Department of Energy Systems Engineering, Yalova-Türkiye
[2]ORCID: https://orcid.org/0009-0005-0815-2580

Yusuf KAYA[3]

[3]Yalova University, Faculty of Engineering, Department of Energy Systems Engineering, Yalova-Türkiye
[3]ORCID: https://orcid.org/0009-0004-1949-7501

Sümeyra İBİŞ[4]

[4]Yalova University, Faculty of Engineering, Department of Energy Systems Engineering, Yalova-Türkiye
[4]ORCID: https://orcid.org/0009-0001-3268-5863

Abstract

The growing global energy demand and the need for a transition to sustainable energy, combined with the environmental impacts and limited resources of traditional fossil fuels, have significantly increased interest in renewable energy sources. In this context, hybrid energy systems offer environmentally and economically efficient solutions. This study aims to simulate and optimize on-grid and off-grid hybrid energy systems using HOMER software to meet the energy consumption of a public building in 2024. By analyzing energy production and storage components such as photovoltaic panels, wind turbines, hydrogen tanks, batteries, thermal boilers, and generators under three different scenarios, the most efficient and cost-effective system designs were identified. In the grid-connected system, Scenario 1 was determined as the optimal solution with a net present cost (NPC) of $10.8 million and a levelized cost of energy (LCOE) of $0.0764/kWh, generating 51.2% of the energy from renewable sources. For those prioritizing energy independence, Off-grid Scenario 1 emerged as a viable alternative with a NPC of $25.3 million and an LCOE of $0.304/kWh. In off-grid scenarios, the use of fossil fuel generators, such as natural gas, reduces renewable energy integration while improving energy security.

This study emphasizes the necessity of conducting comprehensive feasibility assessments when implementing hybrid energy systems and ensuring that system configurations are optimized based on regional energy potential and load demands. Furthermore, integrating additional components, such as electric vehicle charging stations and thermal loads, enhances both system efficiency and flexibility. The findings demonstrate that utilizing renewable energy sources not only increases economic efficiency but also significantly reduces carbon emissions, thus contributing to environmental sustainability.

Keywords: Electrical vehicle charging stations, Hybrid energy systems, Energy efficiency, Cost optimization, Carbon emissions.

Introduction

In the 21st century, the energy sector is undergoing a profound transformation, with sustainability at the forefront of global efforts to mitigate the adverse effects of climate change. The finite nature of fossil fuel reserves, combined with their significant environmental impacts, has intensified the global shift toward renewable energy solutions (Al-Sahlawi et al., 2024). The rising global energy demand, coupled with the urgent need to reduce carbon emissions, underscores the critical importance of Hybrid Renewable Energy Systems (HRES) in addressing these challenges. HRES, which integrate multiple renewable energy sources and advanced storage technologies, offer a reliable and resilient energy supply, overcoming the intermittent nature of solar and wind power (Belkhier et al., 2024).

Hybrid systems enhance energy efficiency by combining diverse renewable sources, such as solar photovoltaics, wind, and biomass, thereby reducing reliance on a single energy source and mitigating fluctuations in power generation (Güven &Yücel , 2024). Additionally, the integration of energy storage technologies, such as batteries and hydrogen storage systems, further strengthens the stability and reliability of these systems. As a result, HRES are increasingly being regarded as a key solution for improving energy security while minimizing environmental impacts and operational costs.

The design and optimization of HRES is a multifaceted challenge that requires advanced computational tools to simulate and optimize system configurations. One of the most widely used tools in this context is HOMER Pro (Hybrid Optimization of Multiple Energy Resources), which enables the simulation of complex energy systems by incorporating various renewable energy sources, storage technologies, and system constraints (Güven & Yörükeren, 2024). Numerous studies have demonstrated that optimizing hybrid energy systems using HOMER Pro can significantly reduce operational costs while enhancing overall system performance (Güven & Yörükeren, 2022).

This study aims to design and optimize HRESs for public buildings with the goal of enhancing energy security and promoting sustainable practices. By using HOMER Pro to simulate scenarios that incorporate photovoltaic panels (PVPs), wind turbines (WTs), hydrogen storage systems, electrolyzers, and batteries, this study aims to identify the most cost effective and efficient configurations for public infrastructure. The primary focus is to optimize energy efficiency and economic feasibility while ensuring that public facilities benefit from stable and sustainable energy sources.

Previous research has demonstrated the notable economic and environmental benefits of hybrid energy systems for public infrastructure. For instance, the impacts of different types of battery impacts on energy storage systems in standalone hybrid renewable energy systems have significantly improved energy reliability and cost efficiency (Güven et al., 2023). Similarly, an optimization and cost analysis of meeting the energy needs of Bahçelievler municipal office using solar and wind systems revealed substantial reductions in operational costs while promoting renewable energy integration (Güven, 2017). These findings underscore the potential of hybrid renewable energy systems to support both economic and environmental sustainability in public infrastructure.

This study expands on the existing literature by assessing the techno-economic viability of hybrid energy systems for public buildings under various scenarios. The results are expected to provide actionable insights into the design and implementation of sustainable energy solutions for public infrastructure, contributing to the broader goals of energy security and environmental stewardship.

Materials and Methods

Selected Location

This study will be conducted at a new public building located 5.5 km from the center of Yalova, a city in Turkey’s Marmara Region (40° 63' 28" N, 29° 26' 62" E). The building, situated on a 200-acre plot of land, features a total indoor area of 105,000 square meters and includes a parking lot with a capacity for 800 vehicles.

Solar Energy Potential

The energy produced by PVPs is directly related to the meteorological data of the region. In this study, the solar energy data for the study area were obtained from the Yalova Meteorological General Directorate database. As shown in Figure 1, the solar energy potential of the region peaks in summer and decreases significantly in winter. The annual average daily solar energy potential was determined as 4205.01 kWh/m²/day. These data are crucial for accurately calculating the efficiency and energy production capacity of PVPs (Güven & Yücel, 2023).

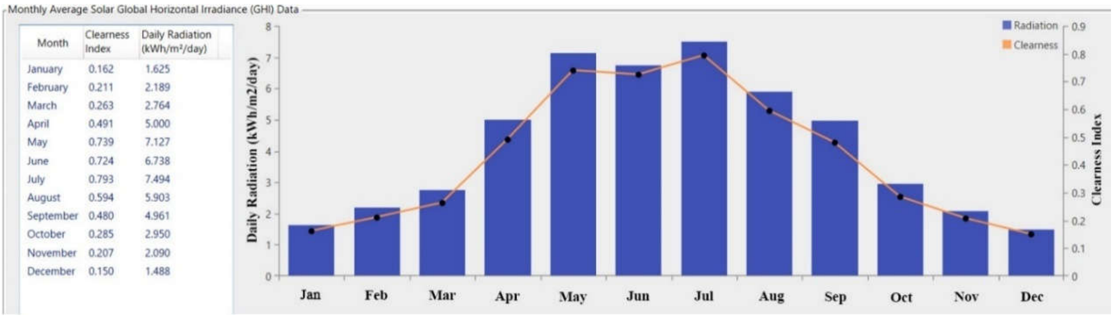

Figure 1. Monthly average solar radiation (kWh/m2/day) profile data for the region

Wind Speed

Due to the high investment costs of WTs, the wind speed profile of the region must be considered. The wind speed profile for this study was obtained from the Yalova Meteorological General Directorate, with an average wind speed of 1.99 m/s. Wind energy is considered a complementary source, especially during winter when solar energy is insufficient. Solar and wind energy are the most common sources of energy in hybrid energy systems. Figure 2 shows the region's detailed wind speed profile, which is vital for evaluating the efficiency and potential energy production of WTs (Güven & Poyraz, 2021).

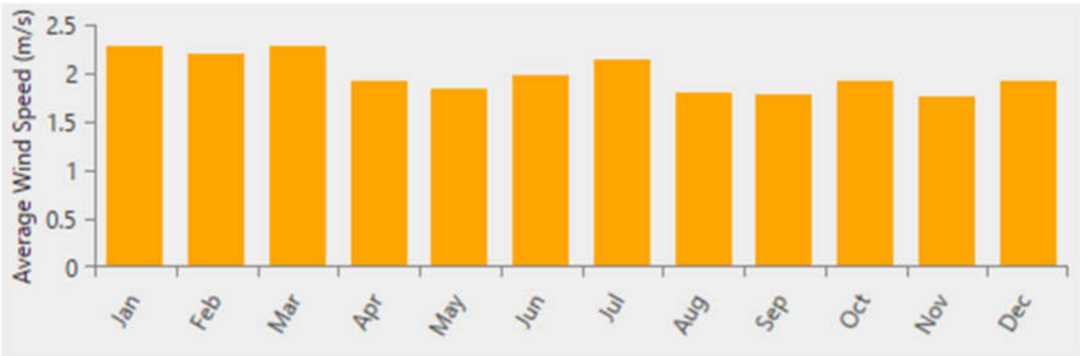

Figure 2. Monthly average wind speed (m/s) profiles of the region

Temperature

The daily temperature values shown in Figure 3 reflect the changes in the climate throughout the year. The data show significant seasonal variations, with temperatures averaging around 5°C in January and rising gradually through summer to peak above 25°C in July and August. The temperature then declines in autumn, dropping to around 10°C in December. These temperature data provide valuable information for evaluating energy system performance and managing energy demand, as the effectiveness of solar and wind energy systems can vary throughout the year due to temperature changes (Güven & Hatipoğlu, 2022).

Figure 3. Annual average temperature data

Electricity Load Profile

The consumption values of the public buildings were obtained from a comprehensive analysis conducted by a research team at the end of 2023. This report examines public buildings' energy consumption patterns, water usage, and other critical resources. It also provided recommendations for improving the building's operational efficiency and achieving sustainability goals. The report highlights potential energy-saving and cost-reduction opportunities during a building's daily operations. The daily load profile exhibited a peak of 974.26 kW at 10:00-AM and a minimum of 421.39 kW at 12:00-AM.

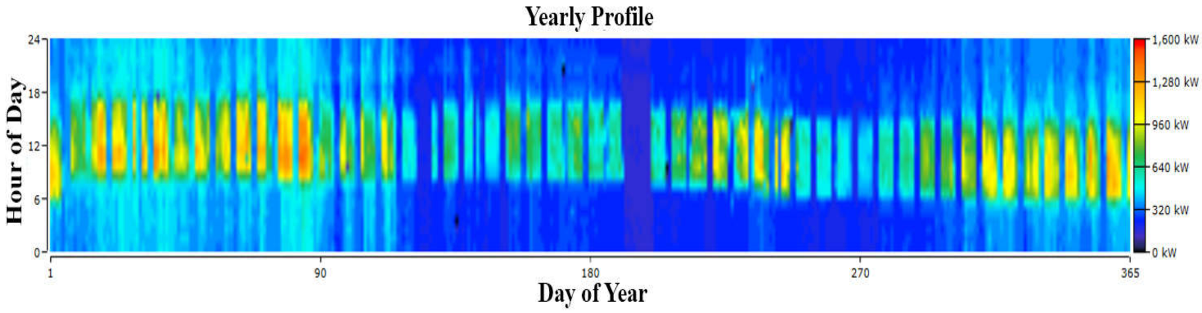

a)

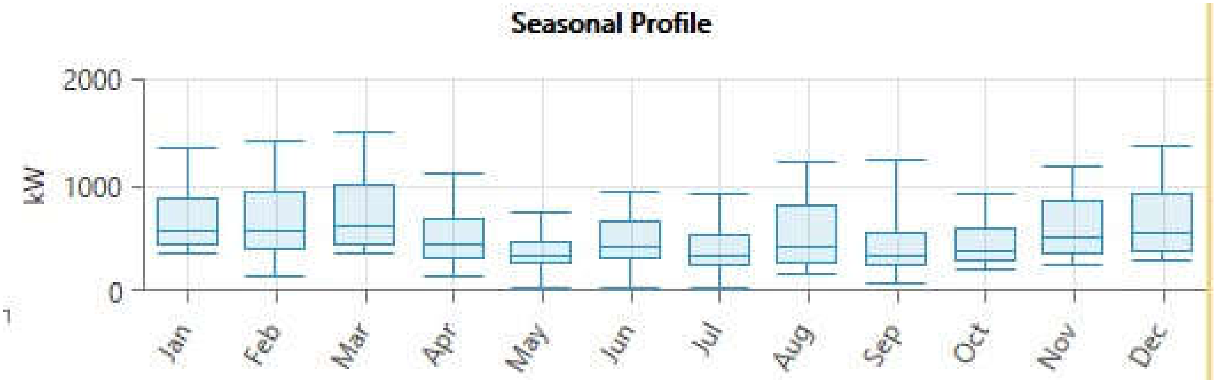

b)

c)

Figure 4. Electricity load profiles (a) annually, (b) seasonal, and (c) daily

Thermal Load Profile

The thermal load profile of the public building in Yalova was examined in detail. The hourly load data for January vary from 429.01 to 659.99 kW. The average daily thermal load consumption was calculated as

6,858.8 kWh/day, with an hourly average of 285.79 kW. These data highlight the thermal load required to meet the building's energy needs. The highest thermal load recorded was 889.89 kW, mainly during winter. The seasonal profiles exhibit fluctuations in thermal load consumption throughout the year, with higher loads in winter and lower loads in summer.

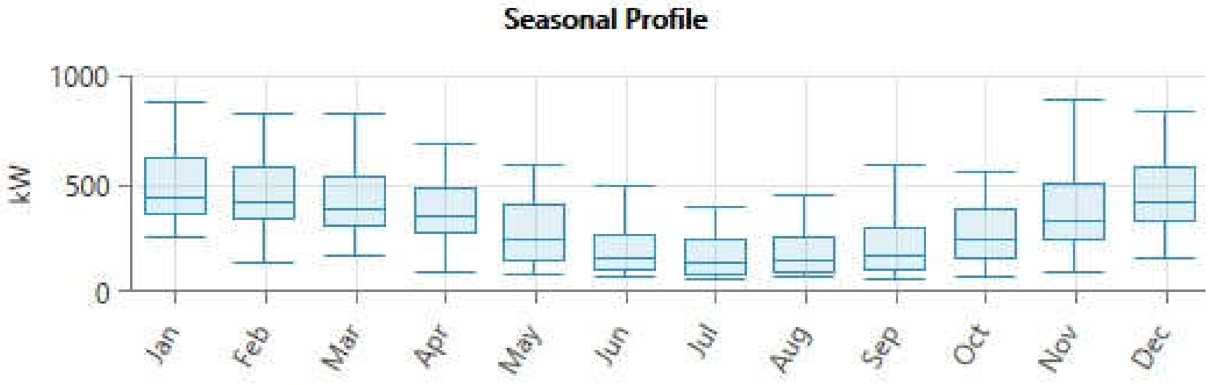

a)

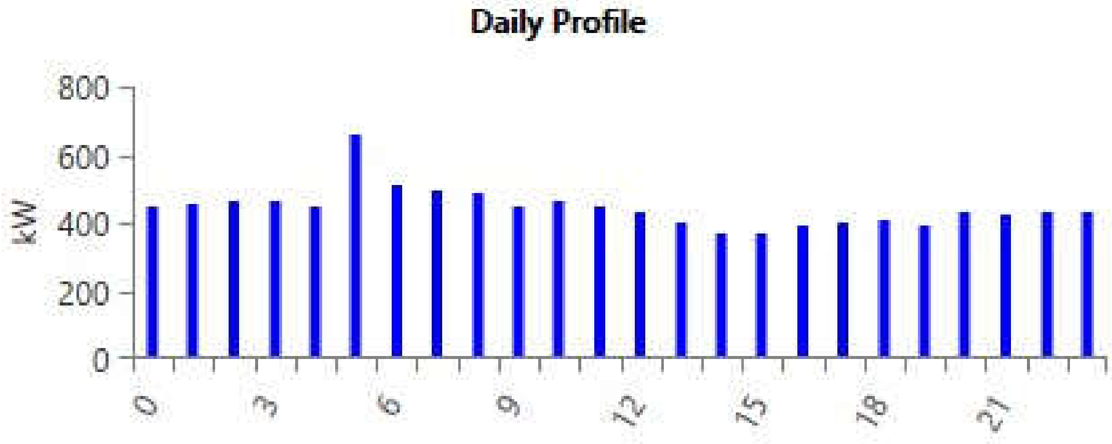

b)

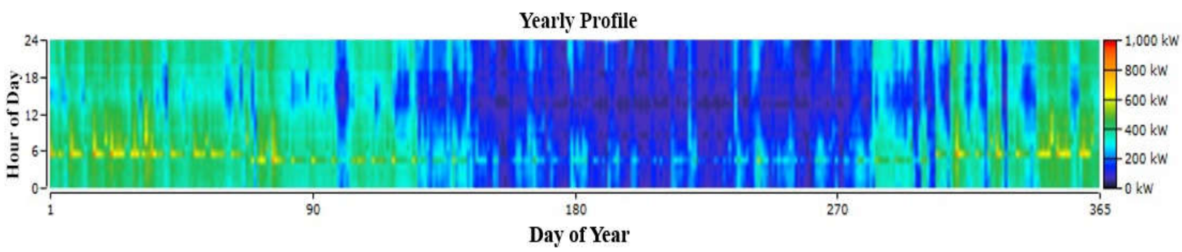

c)

Figure 5. Thermal load profiles: a) seasonal, b) daily, and c) annual

Hydrogen Load Profile

In the hydrogen load model, daily and seasonal profiles were analyzed to determine hydrogen consumption patterns. According to the January profile, the hourly hydrogen load varied between 0.095 and 0.550 kg/h. The average daily hydrogen consumption was 11.26 kg/day, with an hourly average of 0.47 kg/h. These values serve as the baseline for evaluating the overall system performance. The highest hydrogen load was 2.09 kg/h, which typically occurs during specific times of the day. The annual profile shows that hydrogen consumption is stable throughout the year, with a load factor of 0.22.

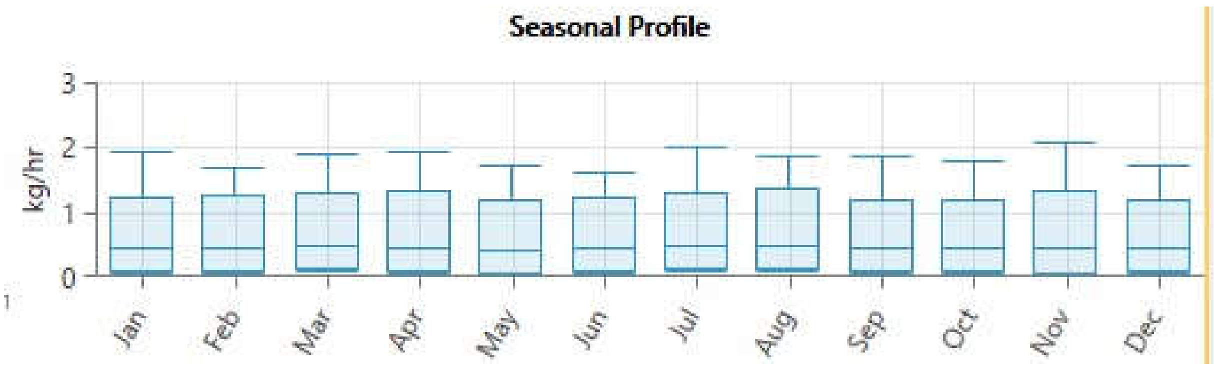

a)

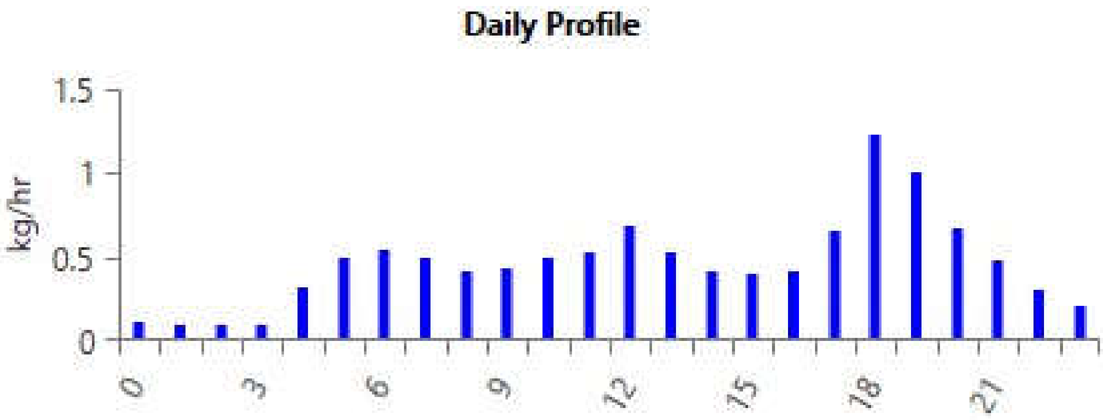

b)

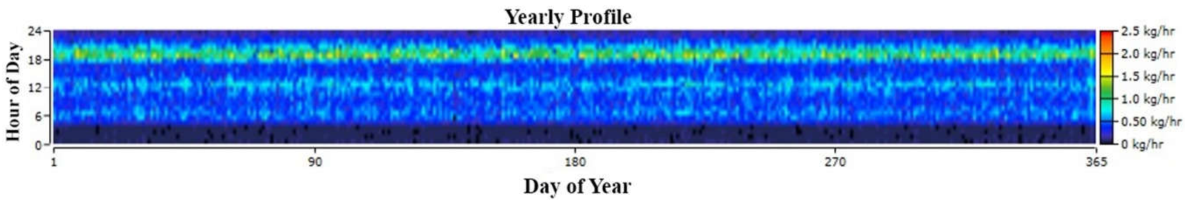

c)

Figure 6. Hydrogen load profiles: a) seasonal, b) daily, and c) annual

Electric Vehicle Charging Station Load Profile

According to the load profile of the EV charging station, the base scenario assumes an average load of 300 kWh/day. Throughout the year, from January to December, the daily average load remains constant at 300 kWh/day, indicating that the station's energy consumption is stable and consistent year-round. The annual average load was calculated as 300 kWh/day. The storage capacity of the charging station was set at 600 kWh, and the maximum load was recorded as 600 kW. The minimum load rate was 20%, indicating that the station maintained a certain level of load during periods of low demand (Güven, 2024a).

Figure 7. Annual average eV charger load data

Hybrid Renewable Energy System Modelling

Figure 8 illustrates the general system configuration of the considered scenarios. In this microgrid structure, key components are connected through both AC and DC busses to ensure flexibility and reliability in energy management (Chowdhury et al., 2023). The gasoline generator, wind turbine, and grid are integrated into the AC bus, which supplies power to the electric load, including the EV charger. The PVPs and battery are connected to the DC bus, which also supplies the electrolyzer that produces hydrogen stored in the hydrogen tank. The hydrogen load is fed directly from the tank, ensuring a continuous supply of hydrogen as needed.

The electric load is primarily connected to the AC bus, while the EV charger has the capability to draw power from both AC and DC busses, enhancing operational flexibility. Additionally, the boiler, which is connected to the AC bus, provides thermal energy. In alternative scenarios, the gasoline generator and boiler can be replaced with diesel or natural gas generators, depending on fuel availability and environmental considerations.

This hybrid system, incorporating both renewable sources like wind and solar power along with energy storage technologies, ensures stability in power supply by addressing the intermittency of renewable energy sources (Diaf et al., 2008). The integration of an electrolyzer and hydrogen storage further enhances the system's capability by storing excess renewable energy in the form of hydrogen, which can later be converted back into electricity or used directly as fuel. The microgrid configuration is designed to optimize energy distribution while minimizing dependency on external grid power, thus improving energy security and sustainability.

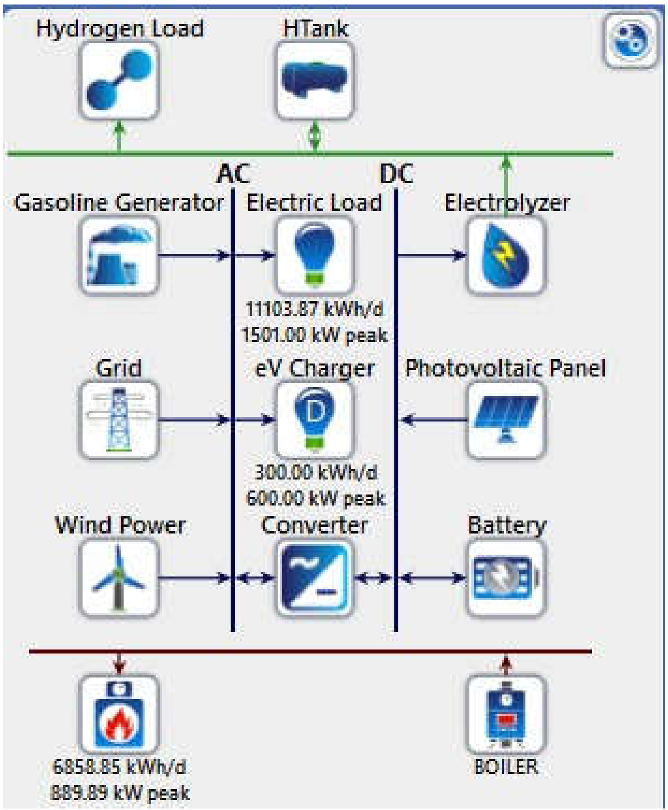

Figure 8. General scenario system configuration

Photovoltaic Panel

In the designed hybrid energy system models, SunPower E20-327 PVPs were selected for their high efficiency and reliability. These PVPs exhibit an efficiency of approximately 20.4% and an expected operational lifespan of approximately 25 years. Each panel has a nominal capacity of 0.327 kW, making it suitable for high-performance applications in renewable energy systems. The initial capital cost of the PV system was estimated to be $1,300 per kilowatt, with the same amount set aside for replacement costs. Additionally, the annual operation and maintenance (O&M) costs are projected to be $20 per kilowatt. The degradation factor of the PV array was approximately 88%, and the ground reflectance was set to 20%, indicating that the panels operated without a tracking system. Capacity adjustments for the PV array were optimized using HOMER.

The power generation from the PVPs can be calculated using the following equation:

$$P_{PV} = Y_{PV} \times f_{PV} \times \left(\frac{G_T}{G_{T.STC}}\right) \times [1 + \alpha_f \times (T_C - T_{C.STC})] \quad (1)$$

In Eq. (1), P_{PV} (kW) represents the output power of the PV array during the specified time interval. Y_{PV} (kW) is the rated output power of the PV panel under the Standard Test Conditions (STC), while f_{PV} (%) denotes the degradation factor of the PV system. G_T (kW/m²) refers to the solar irradiance incident on the PV array during the specified time interval, and $G_{T.STC}$ (1 kW/m²) represents the solar irradiance under the STC (which assumes an ambient temperature of 25°C). The term α_f (%/°C) is the temperature coefficient of the PV panel, reflecting how the panel's performance changes with temperature. T_C (°C) is the PV panel temperature during the time interval, while $T_{C.STC}$ (°C) represents the PV panel temperature under STC conditions (typically 25°C).

If the temperature effect on the PV panel (α_f) is not considered in HOMER software, the simplified calculation for the PV power output can be represented by equation (2):

$$P_{PV} = Y_{PV} \times f_{PV} \times \left(\frac{G_T}{G_{T.STC}}\right) \quad (2)$$

This simplified equation disregards the impact of temperature on the PV system, assuming ideal conditions modeled by the HOMER tool. However, in real-world scenarios, the influence of temperature can significantly affect the efficiency and output of PVPs, particularly in regions with extreme climatic conditions (Güven & Mete, 2021).

Wind Turbine

In the proposed models, the wind turbine is designed with specialized blades to capture the kinetic energy generated by the wind. As the wind passes over the blades at a suitable height, a lift force is generated, which causes the blades to rotate. These blades are connected to a drive shaft, which in turn rotates a generator to produce electricity.

The EOCYCLE E020 wind turbine was selected for the model owing to its optimal performance under various wind conditions. This turbine has a cut-in and cut-out wind speeds of approximately 2.75 and 20 m/s. The rotor diameter was 15.81 m, providing a significant swept area for energy capture. The capital cost of the wind turbine is estimated to be $50,000 per kilowatt, with a replacement cost of $35,000. The annual operation and maintenance (O&M) costs are projected to be $50. The power capacity of the turbine is approximately 20 kW, and it has a total operational lifespan of about 25 years. The turbine can be installed on hydraulic towers with hub heights of 16 or 23 m, or on non-hydraulic towers with hub heights of 30 or 36 m, depending on the site-specific requirements.

HOMER Pro software was used to calculate the wind turbine power output in three stages. First, the wind speed at the hub height is calculated using the equation below. Based on the calculated wind speed under the Standard Test Conditions (STC), the expected power output from the wind turbine was estimated using the power curve shown in Figure 9. Finally, HOMER Pro adjusts the predicted power output by factoring in the air density ratio, as shown in equation (4), to calculate the actual power output facilitated by the wind turbine under real-world conditions.

$$U_{hub} = U_{anem} \times \frac{\ln\left(\frac{Z_{hub}}{Z_0}\right)}{\ln\left(\frac{Z_{anem}}{Z_0}\right)} \quad (3)$$

In Eq. (3), U_{hub} (m/s) represents the wind speed at the wind turbine hub height, while U_{anem} (m/s) refers to the wind speed at the anemometer height. Z_{hub} (m) is the hub height of the wind turbine, and Z_{anem} (m) is the height of the anemometer. Z_0 (m) is the surface roughness length, which reflects the terrain characteristics.

The wind turbine power output is then calculated as Eq.(4):

$$P_{WTG} = \left(\frac{\rho}{\rho_0}\right) \times P_{WTG,STC} \quad (4)$$

In Eq. (4), P_{WTG} represents the actual power output of the wind turbine, adjusted for air density, where ρ is the actual air density at the site, and ρ_0 is the air density under standard conditions. $P_{WTG,STC}$ is the power output of the wind turbine under standard conditions (STC). This adjustment ensures that the calculated power output aligns with the real operating conditions, as the air density can vary significantly depending on temperature, altitude, and weather conditions (Güven & Mengi, 2023).

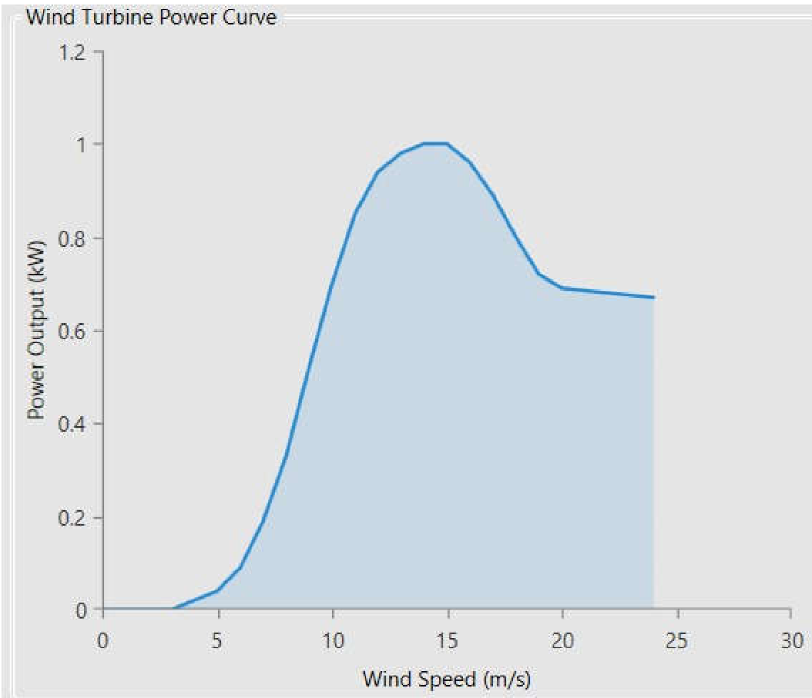

Figure 9. Wind power curve

System Generator

For the design and simulation of the project, an Autosize Genset generator was utilized, which was optimized according to the system requirements using HOMER Pro software. The generator operates with a minimum load ratio of 25%, and its expected lifespan is approximately 15,000 hours. The capital, replacement, and operational costs are estimated at $500, $500, and $0.030 per hour, respectively. The generator is modeled under six different scenarios, employing three distinct fuel types: diesel, natural gas, and gasoline. The fuel consumption rate was calculated based on the generator's power output using equation (5):

$$F(t) = (F_0 \times Y_{gen}) + (F_1 \times P_{gen}) \quad (5)$$

In Eq. (5), $F(t)$ represents the fuel consumption rate of the generator, F_0 (L/h/kW) is the intercept of the fuel consumption curve, F_1 (L/h/kW) is the slope of the fuel consumption curve, Y_{gen} (kW) is the nominal power of the generator under the Standard Test Conditions (STC), and P_{gen} (kW) represents the actual output power of the generator during the time interval (Güven, 2024b).

The overall efficiency of the generator can be calculated using the following equation:

$$\eta_G = \left(\frac{3{,}6 \times X_G \times P_{gen}}{m_f \times LHV_f}\right) \quad (6)$$

This efficiency equation (6) defines the ratio of the generator's electrical output to its fuel input, where X_G is the energy conversion factor, m_f is the mass flow rate of the fuel, and LHV_f is the lower heating value of the fuel (Hasanien et al., 2024).

Diesel Generator

Diesel generators operate by compressing and igniting diesel fuel, which drives the engine pistons to produce mechanical energy that is then converted into electricity by the generator. For the generator used in this project, three fuel prices were considered for the sensitivity analysis: $1.34, $1.50, and $1.75 per liter. These variable prices are key factors in evaluating the operational costs of generators and were analyzed in the sensitivity analysis section.

Natural Gas Generator

Natural gas generators work by compressing and igniting natural gas in the combustion chamber, which produces the mechanical energy needed to generate electricity. For the natural gas generator used in this project, three fuel prices were considered: \$0.143, \$0.17, and \$0.20 per cubic meter. These prices directly affect the operational costs of generators and are critical to the economic analysis of the system.

Gasoline Generator

Gasoline generators operate by igniting gasoline fuel through a spark plug, where the fuel is compressed in the engine's cylinders and ignited by the spark plug to generate mechanical energy. For the gasoline generator used in this project, three fuel prices were considered: \$1.38, \$1.45, and \$1.65 per liter. As with other fuel types, these variable prices affect the overall operating costs and were considered in the sensitivity analysis.

Battery Storage System

The battery used in the proposed model is a kinetic battery with a nominal voltage of 6 V and a nominal capacity of 6.91 kWh. The maximum capacity is 1150 Ah, and the capacity ratio is 0.237. The round-trip efficiency of the battery was approximately 80%, with maximum charge and discharge currents of 279 amperes. The specific model used in this project is a 6 CS 25P battery with a capacity of 820 Ah and an operational lifespan of 12 to 20 years. The capital cost of the battery was \$1,100, with a replacement cost of \$1,000 and annual O&M cost of \$20. The battery is expected to be last 15 years and provide a total energy throughput of approximately 6,879.60 kWh over its lifetime. The initial state of charge is set to 100%, and the minimum allowable state of charge is 40%.

The number of batteries required for the system was calculated using the following Eq. (7):

$$N_{bat} = \frac{E_d \times n_d}{V_{bat} \times Ah \times DD} \quad (7)$$

In Eq. (7), E_d (kWh) represents the daily energy demand, n_d refers to the number of autonomous days, V_{bat} (V) is the battery voltage, Ah is the battery capacity, and DD (%) is the depth of discharge. This calculation helps determine the appropriate battery size to meet the energy storage needs of the system based on the energy demand and operational conditions (Jui et al., 2024).

Electrolyzer

The "Generic Electrolyzer" model is used in the design of this system. In the electrolyzer, water is split into hydrogen and oxygen molecules via electrolysis. The hydrogen produced during this process is used to generate electricity. The capital and replacement costs for a 1-kW electrolyzer are estimated to be \$150, with an operational cost of \$8 per kilowatt. The lifespan of the electrolyzer was set at 15 years, and its efficiency was simulated under two different sensitivity levels: 85% and 67.5%. The chemical reactions occurring in the electrolyzer are presented below:

Overall chemical reaction:

$$2H_2O \rightarrow 2H_2 + O_2 \quad (8)$$

Reaction at the anode:

$$4OH^- \rightarrow 2H_2O + O_2 + 4e_- \quad (9)$$

Reaction at the cathode:

$$4H_2O + 4e_- \rightarrow 2H_2^+ + 4OH^- \quad (10)$$

Numerical modeling of the electrolyzer is an effective technique for evaluating cell performance and the complex physicochemical processes involved, including the electrochemical reactions and mass transport at the cathode and anode. The model also incorporates the thermodynamics of the system and losses in the electrical circuits. The reversible cell voltage under the standard temperature and pressure (STP) conditions,

U_{revs}^{STP}, is determined by the thermodynamics of the water-splitting reaction at STP and can be calculated as follows:

$$U_{revs}^{STP} = \frac{-\Delta G^{STP}}{nF} = U_{revs}^{STP^0} + \frac{RT}{nF} \times ln\left[(p - \rho_w)^{1.5} \times \frac{\rho_w^*}{\rho_w}\right] \quad (11)$$

Here, ΔG^{STP} is the Gibbs free energy, FFF is the Faraday constant, and n is the number of electrons involved in the electrode reaction. ρ_w is the partial pressure of pure water, while ρ_w^* is the partial pressure of the gaseous electrolyte. The RRR is the universal gas constant (8.315 J/mol·K), and T is the temperature in Kelvin. U_{revs}^{STP} represents the reversible cell voltage under given STP conditions and can be determined as:

$$U_{revs}^{STP^0} = 1.50342 - 9.956 \times 10^{-4} \times T + 2.5 \times 10^{-7} \times T^2 \quad (12)$$

The values of ρ_w and ρ_w^* can be calculated as follows:

$$\rho_w = \exp\left(37,93 - \frac{6426,32}{T}\right) \times \exp\left(0,016214 - 0,13802 + (0,19330 \times \sqrt{M}\right) \times T^{-3,498} \quad (13)$$

$$\rho_w^* = exp\left(377,93 - \frac{6426.32}{T}\right)T^{-3.498} \quad (14)$$

The Butler-Volmer equation is used to determine the cell current density (j_{cell}) and is given as

$$j_{cell} = j_0[\exp\left(\frac{\alpha}{RT} \times n \times F \times U_{act}\right) - \exp\left(\frac{(1-\alpha)}{RT}\right) \times n \times F \times U_{act} \quad (15)$$

In this equation, j_0 represents the exchange current density at equilibrium, and α\alphaα is the charge transfer coefficient, which quantifies the proportion of the energy barrier between the electrodes. The activation overpotential U_{act} is the sum of the anode and cathode overpotential voltages, which is calculated using the Tafel equation (16):

$$U_{act} = U_{act}^a + U_{act}^c = 2,3026 \times \frac{RT}{n \times F \times \propto_a} \times \log\left(\frac{j}{j_{0-a}}\right) + 2,3026 \times \frac{RT}{n \times F \times \propto_c} \times \log\left(\frac{j}{j_{0-c}}\right) \quad (16)$$

The exchange current density of the cell depends on the roughness and geometry of the electrode material. The charge transfer coefficients $\propto_c$ and $\propto_a$ typically range between 0.2 and 0.8, although experimental models reported in the literature suggest that the values of $\propto_c$ and $\propto_a$ are generally between 0.67 and 0.70.

Hydrogen Tank

The hydrogen tank is used for storing hydrogen, which is later used to power fuel cells. The capital cost of the hydrogen tank was estimated to be $1.5 per kilogram of storage capacity, with a similar replacement cost of $1.5 per kilogram. The annual operation and maintenance (O&M) cost is projected to be $8. The tank's storage capacity ranges from 1 to 300 kg, allowing flexibility in the system design depending on the energy requirements. The lifespan of the hydrogen tank was carefully selected to be 25 years to ensure long-term durability and reliability (Nandi et al., 2024).

Boiler

A Generic Boiler model has been implemented in the project, operating with 85% efficiency and fueled by natural gas. The lower heating value (LHV) of natural gas was 45 MJ/kg, and its density was 0.790 kg/m³. When fueled with natural gas, the boiler produces relatively low emissions of carbon monoxide, unburned hydrocarbons, particulate matter, sulfur, and nitrogen oxides. The boiler was simulated under various scenarios using natural gas, gasoline, and diesel as fuel sources, each with distinct emission and cost profiles.

Sensitivity analysis was performed using varying fuel prices: gasoline prices were set at $1.38/L, $1.45/L, and $1.65/L; natural gas prices were set at $0.143/m³, $0.17/m³, and $0.20/m³; and diesel prices were set at $1.34/L, $1.50/L, and $1.75/L. The impact of each fuel on the operational cost and boiler performance was evaluated. Fossil fuels such as gasoline and diesel produced higher emissions because of their higher carbon content than natural gas. These analyses are critical for understanding the boiler efficiency and environmental impact of using different fuel types.

The influence of fuel prices on the boiler's operational costs was also considered, enabling the identification of the most cost-effective and environmentally friendly option. By performing these calculations, it is ensured that both the electric and gas boilers efficiently meet the required thermal demand. The equation below outlines the energy balance of the boiler system:

$$E_{Boiler}(t) = E_{thermal}(t) - [E_{BES} + E_{REH}(t) + (E_{TES}(t-1) \times (1-\varphi) - E_{TES,min} \quad (17)$$

This equation (17) represents the energy required by the boiler at time t, where $E_{thermal}(t)$ is the thermal energy demand at time t, E_{BES} is the energy storage from the battery, $E_{REH}(t)$ is the energy recovery at time t, $E_{TES}(t-1)$ is the thermal energy stored at the previous time step, and φ is the thermal storage efficiency. $E_{TES,min}$ represents the minimum energy required for thermal energy storage.

Grid System

In the HOMER Pro simulation of a grid-connected system, electricity pricing and sale rates vary depending on the time of day. The T3 peak electricity pricing structure in Turkey has been integrated into this system. Rate 1, which operates from 06:00 to 17:00, has a cost of $0.1600/kWh and a sale price of $0.1000/kWh. Rate 2, which operates from 17:00 to 22:00, has a cost of $0.1800/kWh and sale price of $0.1000/kWh. Rate 3, which operates from 22:00 to 06:00, has a cost of $0.1200/kWh and sale price of $0.1000/kWh. This pricing structure significantly affects the distribution of energy consumption throughout the day and plays a crucial role in cost optimization. Specifically, the T3 peak pricing implies that electricity use during peak hours incurs higher costs, whereas nighttime energy usage benefits from lower costs. This structure is critical for shaping energy management strategies and optimizing costs.

Converter

A Generic System Converter is utilized in the model, which is integrated into HOMER Pro software. This converter operates in both the inverter and rectifier modes. In situations where solar and wind resources are unavailable, the converter functions in inverter mode, which is typically occurring during nighttime or cloudy conditions. However, when sufficient renewable energy is available, the converter operates in rectifier mode to charge the battery storage system. The efficiency of the converter is approximately 95%. The cost of a 1 kW converter is approximately $300, with a replacement cost of $300 and a lifespan of 15 years.

The inverter capacity within the system can be calculated using the following Eq. (18).

$$P_{inv} = \frac{E_{L,max}}{\eta_{DC/AC}} \quad (18)$$

In Eq. (18), P_{inv} (W) represents the power capacity of the converter, $E_{L,max}$ (Wh) denotes the maximum energy demand required by the load, and $\eta_{DC/AC}$ represents the conversion efficiency (Falope et al., 2024).

Economic Model

Economic models play a pivotal role in making investment decisions, determining operational strategies, and assessing the integration of renewable energy sources. Key economic indicators, such as the annual total cost-saving ratio, NPC, and levelized cost of electricity (LCOE), are commonly used to evaluate the cost-effectiveness of different energy systems and projects. These economic models are critical for the design and implementation of sustainable and efficient energy systems.

Net Present Cost

The NPC of a hybrid system represents the total cost of the system over its defined lifetime, accounting for all associated costs, such as initial capital, replacement, and operation and maintenance (O&M), while subtracting the salvage value at the end of the system's useful life. HOMER Pro software calculates the NPC of each component in the system using the following Eq. (19).

$$NPC = \sum(C_{capital} + C_{replace} + C_{maint} + C_{salvage}) \quad (19)$$

Levelized Cost of Energy (LCOE)

The LCOE is the average cost per kilowatt-hour of electricity produced by a system over its operational lifetime. To calculate LCOE, HOMER Pro divides the total annual cost by the sum of $L_{primeAC}$ and $L_{primeDC}$, as shown in the following Eq. (20) (Okafor et al., 2024).

$$LCOE = \frac{\text{Total Annual Cost}}{L_{primeAC}+L_{primeDC}} \quad (20)$$

Total Annual Cost

The total annual cost represents the yearly value associated with the project over its estimated lifespan, which corresponds to the NPC calculated through HOMER Pro. This value is then multiplied by the capital recovery factor to obtain the final total annual cost.

Annual Total Cost Saving Ratio

The annual total cost-saving ratio is used to assess the cost-effectiveness of a system or process. This ratio reflects the cost savings achieved by implementing a project or system modification. Typically expressed as a percentage, this is calculated by comparing the initial and replacement/maintenance costs:

$$YTMTO\ (\%) = \frac{(\text{Initial Cost}-\text{Replacement CostInitial Cost})}{\text{Initial Cost}} \times 100 \quad (21)$$

Salvage Value

HOMER Pro calculates the salvage value of specific components using the following formula. The salvage value represents the remaining value of the power system component at the end of the project lifecycle. HOMER assumes linear depreciation for a component, meaning that the salvage value is proportional to the remaining lifespan of the component. HOMER specifies that the salvage value is based on the replacement cost rather than the initial capital cost. The salvage value is calculated as follows:

$$S = C_{rep} \times \frac{R_{rep}}{R_{comp}} \quad (22)$$

Environmental Performance Indicators

The environmental performance indicators in HOMER Pro are used to evaluate the environmental impact of energy systems. These indicators include factors such as carbon emissions, fuel consumption, and air pollution. Carbon emissions, in particular, are a key metric for assessing the environmental impact of energy production and are calculated using the following Eq. (23).

$$\text{Carbon Emissions (tons)} = \left(\frac{\text{Fuel Consumption } (liter\ or\ m^3)}{\text{Fuel Efficiency}}\right) \times \text{Emission Factor} \quad (23)$$

Environmental performance indicators are essential for assessing the sustainability of energy systems and their alignment with environmental goals. Minimizing carbon emissions, optimizing fuel consumption, and reducing air pollution are critical objectives for improving environmental performance. This project aims to enhance system efficiency and sustainability by considering these indicators in energy system design. Integrating environmental performance indicators helps optimize energy systems from both an economic and environmental perspective (Sadeghi et al., 2024).

Renewable Energy Fraction

The renewable energy fraction in HOMER Pro represents the proportion of total energy production supplied by renewable energy sources. This ratio is calculated by dividing renewable energy production by total energy production as follows Eq. (24).

$$\text{Renewable Energy Fraction } (\%) = \left(\frac{\text{Renewable Energy Fraction } (kWh)}{\text{Total Energy Production } (kWh)}\right) \times 100 \quad (24)$$

In this project, the renewable energy fraction was not constrained to a specific value, allowing HOMER Pro to optimize the system based on available renewable energy resources. This approach ensures that the system takes full advantage of renewable energy sources while offering a cost-effective solution. HOMER Pro analyzes various scenarios to identify the most efficient configuration while striking an optimal balance between energy sources (Güven & Yörükeren, 2024).

Findings and Discussion

The hybrid energy system designed to meet the 2024 electricity consumption values of a new public building, located 5.5 km from Yalova city center, was created by integrating the components defined in the system components section into the simulation. The optimal simulation results for three grid-connected and three off-grid system scenarios are presented in Table 1.

Table 1. Optimization results for on- grid and off-grid scenarios

Scenario	**PV Panel (kW)**	**Wind Turbine (kW)**	**Generator (kW)**	**Battery(kWh)**	**Converter**	**Electrolyzer (kW)**	**Hydrogen Tank (kg)**	**NPC ($)**	**COE ($/kWh)**
On grid									
1	4000	78	-----------	3	2707	100	300	11,7 M	0,0764
2	4000	78	-----------	--------	2868	100	300	17,7 M	0,0765
3	4000	78	-----------	--------	2868	100	300	18,7 M	0,0765
Off grid									
1	2182	62	2300	527	1130	100	300	25,4 M	0,304
2	4000	208	2300	1818	1892	100	300	48 M	0,499
3	3968	208	2300	1813	1502	100	300	49,1 M	0,502

As shown in Table 1, the grid-connected scenarios use components such as PVPs, WTs, hydrogen tanks, batteries, electrolyzers, and thermal loads. In these scenarios, variations in system components, renewable energy percentages, fuel prices (natural gas, gasoline, diesel), EV charging loads, and the minimum power capacity of EV charging stations were adjusted to determine the optimal system configuration. Similarly, the same components were considered for the off-grid system but with the addition of generators.

In grid-connected scenarios, no generator was used, whereas natural gas, diesel, and gasoline generators were used in off-grid systems. Specifically, off-grid scenario 1 uses a natural gas generator, Scenario 2 employs a diesel generator, and Scenario 3 uses a gasoline generator.

When evaluating the results of these scenarios, grid-connected scenario 1 was determined to be the most cost-effective system, with an NPC of $10.8 million and LCOE of $0.0764 per kWh. This scenario incorporates PVPs, WTs, hydrogen tanks, batteries, electrolyzers, and thermal load components, resulting in an optimal hybrid energy system from a cost perspective.

For off-grid systems, Scenario 1, with a natural gas generator, PVPs, WTs, hydrogen tanks, batteries, electrolyzers, and thermal load components, stands out as the most cost-effective configuration, with an NPC of $25.3 million and COE of $0.304 per kWh.

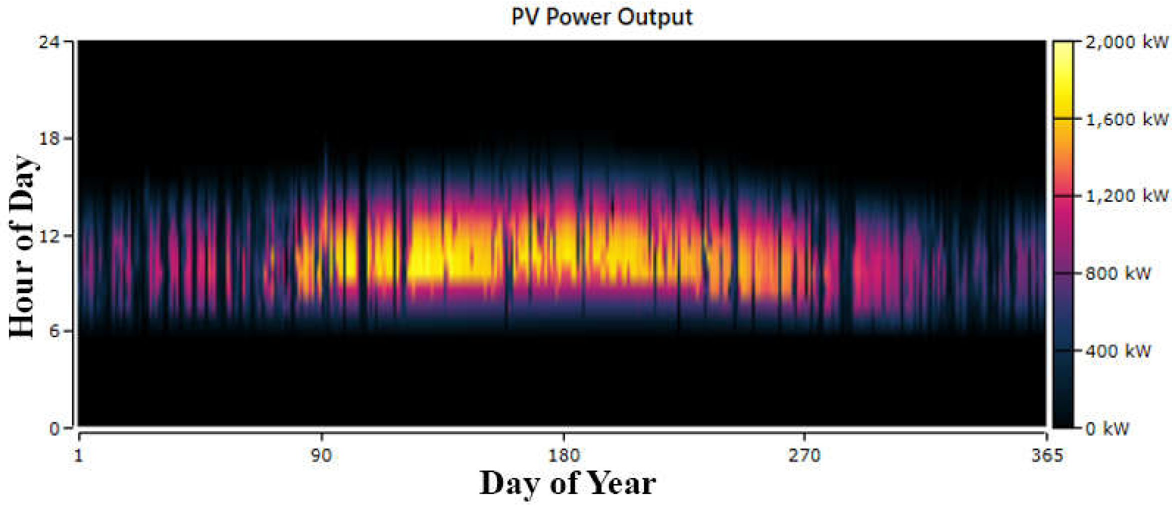

a)

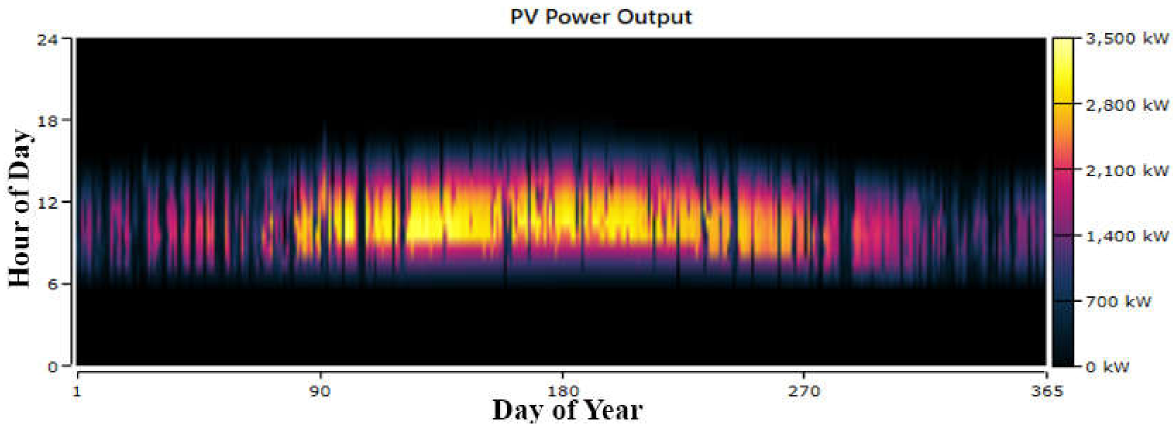

b)

Figure 10. Solar panel output power for (a) off-grid scenario (b) on-grid scenario

In Figure 10 (a), the output power generated by the PVPs in off-grid scenario 1. As expected, the highest efficiency was achieved during midday when the sun's rays hit the Earth most directly and intensely. During winter, there is a noticeable decrease in the output power. The PVPs operate for 3,857 hours annually, generating a total of 2,353,853 kWh/year of electricity. The unit cost of electricity produced by the panels is $0.0808/kWh.

Figure 10 (b), the output power generated by the PVPs in the on-grid scenario is presented. The PVPs operate for 3,857 hours annually, generating a total of 4,314,326 kWh/year of electricity. The unit cost of electricity produced by the panels is $0.0808/kWh.

In Figure 11, the state of charge (SOC) of the batteries in off-grid scenario 1 are shown for different days and hours throughout the year. During the months when the PVPs operate at maximum efficiency (between April and October), the SOC reaches approximately 90% during midday. However, during the other hours of the day, particularly in January, February, March, November, and December, the SOC drops to between 52% and 72%. Despite these fluctuations, the fact that the batteries only reached the minimum SOC during the months with limited sunlight indicates that the system had a sufficient number of batteries to meet the energy demand.

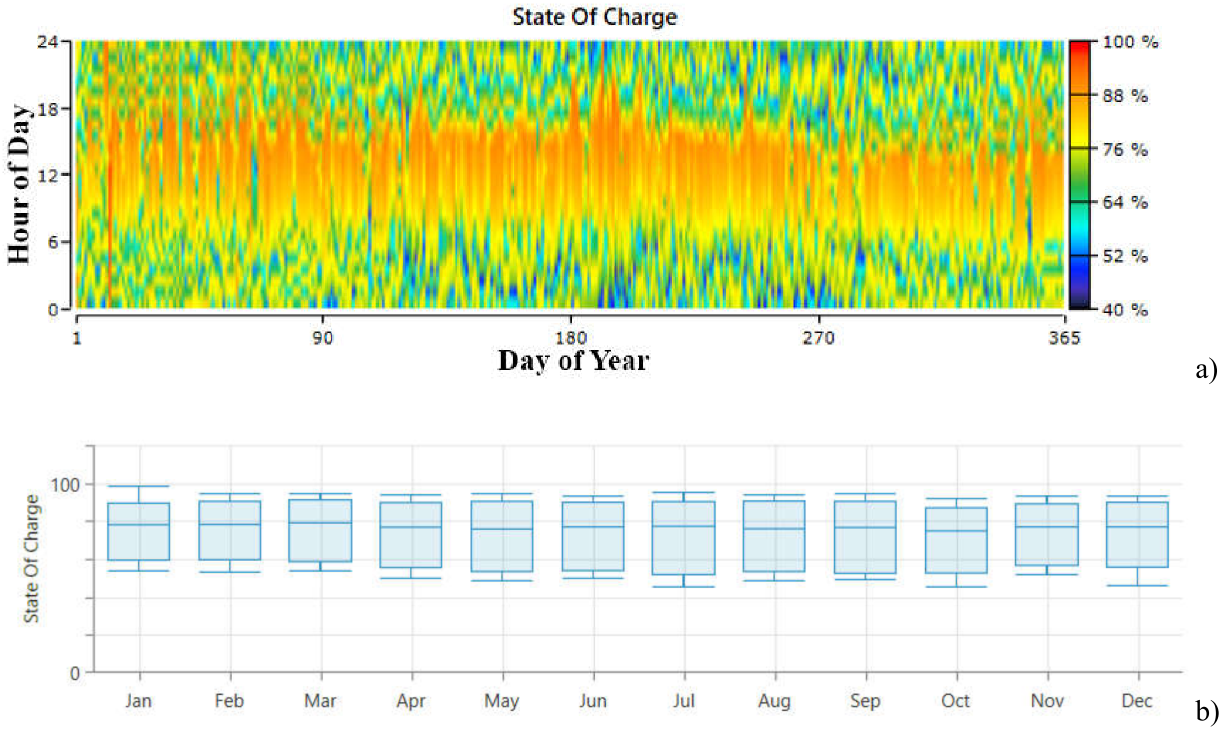

Figure 11. Battery state of charge in off-grid scenario 1 a) daily b) monthly

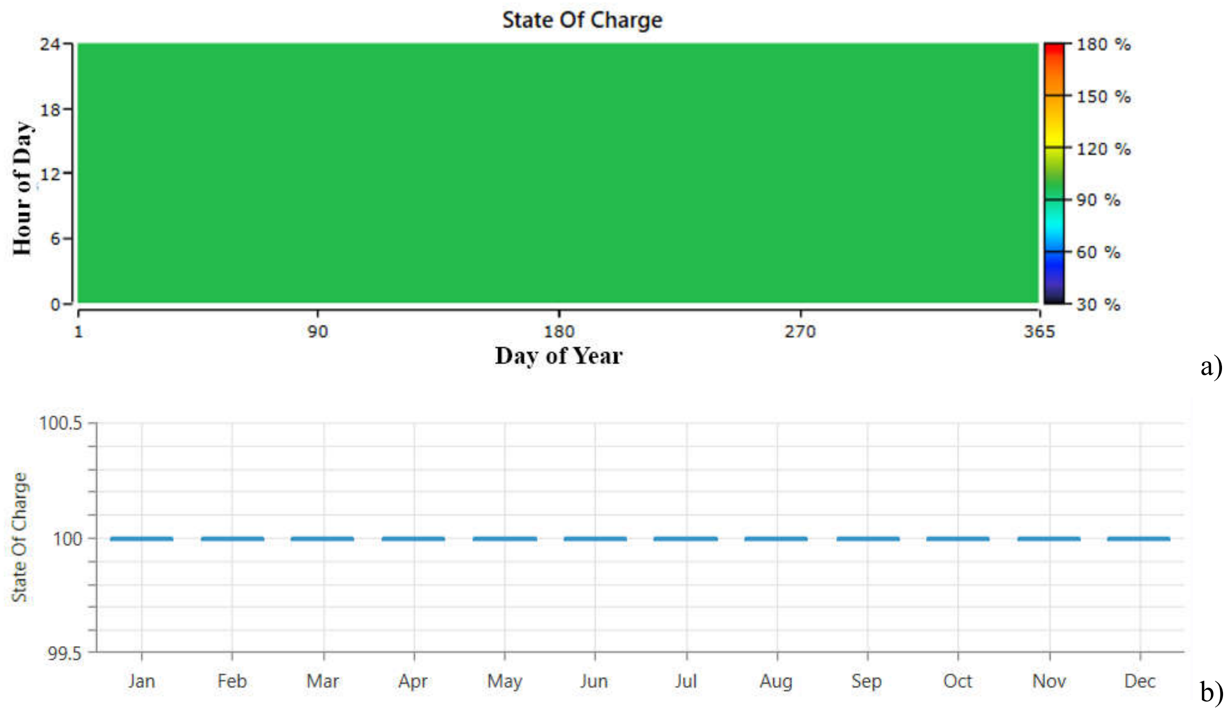

Figure 12. Battery state of charge in on-grid scenario 1 a) daily b) monthly

In Figure 12, the SOC of the batteries used in on-grid Scenario 1 are displayed for different days and hours throughout the year. As shown in the figure, the SOC remained at 100% throughout all months of the year. This is due to the system being connected to the grid, ensuring a constant supply of energy to fully charge the batteries at all times.

In Figure 13, the output power of the natural gas generator used in Scenario 1 is shown for different days and hours throughout the year. As observed in the graph, the integration of batteries and PVPs into the system significantly reduced the dependency on the electricity generated by the natural gas generator. The generator operates for a total of 3,626 hours annually, producing 2,970,246 kWh of electricity. The unit cost of electricity produced by the generator is $0.0367/kWh. Notably, between days 90 and 300 (from 06:00 to 18:00), the generator was scarce. This indicates that sufficient energy is supplied by the PVPs during daylight hours and that energy is drawn from the batteries when the sun is not available.

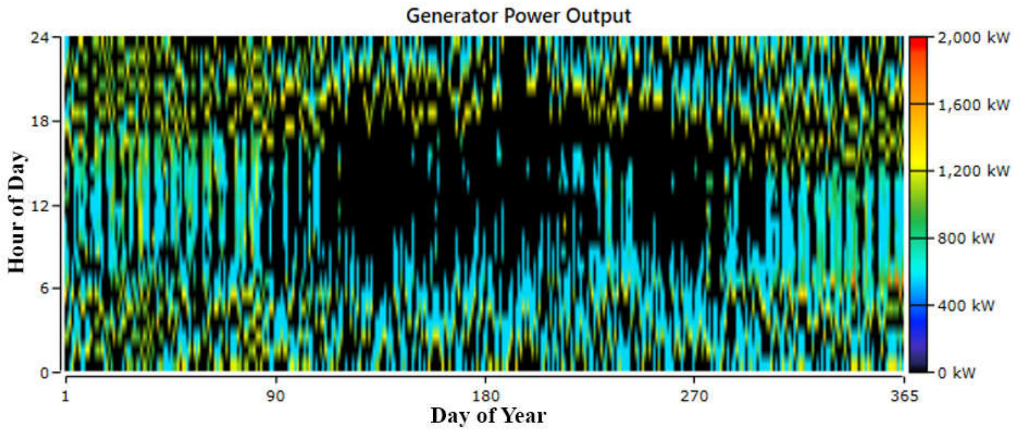

Figure 13. Daily output power of the generator (off-grid)

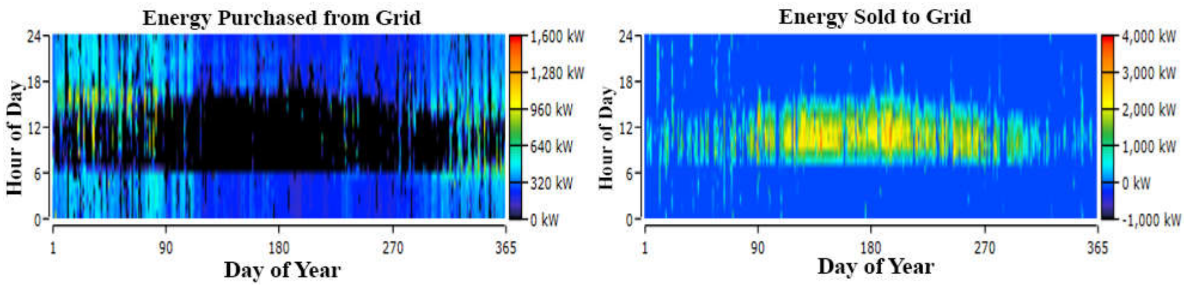

Figure 14. Annual energy purchased from and sold to the grid

In Figure 14, the amounts of electricity purchased from and sold to the grid in Scenario 1 are shown for different times of the year. The system purchased a total of 1,993,654 kWh of energy from the grid over the year and sold a total of 2,556,404 kWh back to the grid. This indicates that the electricity generated by the system components not only met the energy demand most of the time, but there was also a surplus of the electricity produced, which was sold back to the grid. This surplus energy sale contributed to additional system revenues.

Table 2. Electrical energy purchased and sold from the grid

Month	Energy Purchased (kWh)	Energy Sold (kWh)	Net Energy Purchased (kWh)	Peak Load (kW)	Energy Cost ($)	Demand Charge ($)
January	240,841	92,075	148,766	1,295	9,499.14	0
February	214,319	86,024	128,295	1,21	7,978.27	0
March	222,178	123,302	98,876	1,231	3,851.19	0
April	152,226	264,185	-111,959	788	18,819.54	0
May	107,422	416,001	-308,579	397	41,134.14	0
June	120,288	335,563	-215,275	503	30,248.18	0
July	89,762	432,193	-342,431	1,295	44,968.64	0
August	129,441	269,357	-139,916	981	21,623.46	0
September	108,554	281,53	-172,975	661	24,888.99	0
October	137,652	161,175	-23,523	920	8,093.90	0
November	210,413	59,933	150,48	1,273	10,253.51	0
December	260,556	35,066	225,49	1,467	17,617.58	0
Annual	1,993,654	2,556,404	-562,75	1,467	140,577.97	0

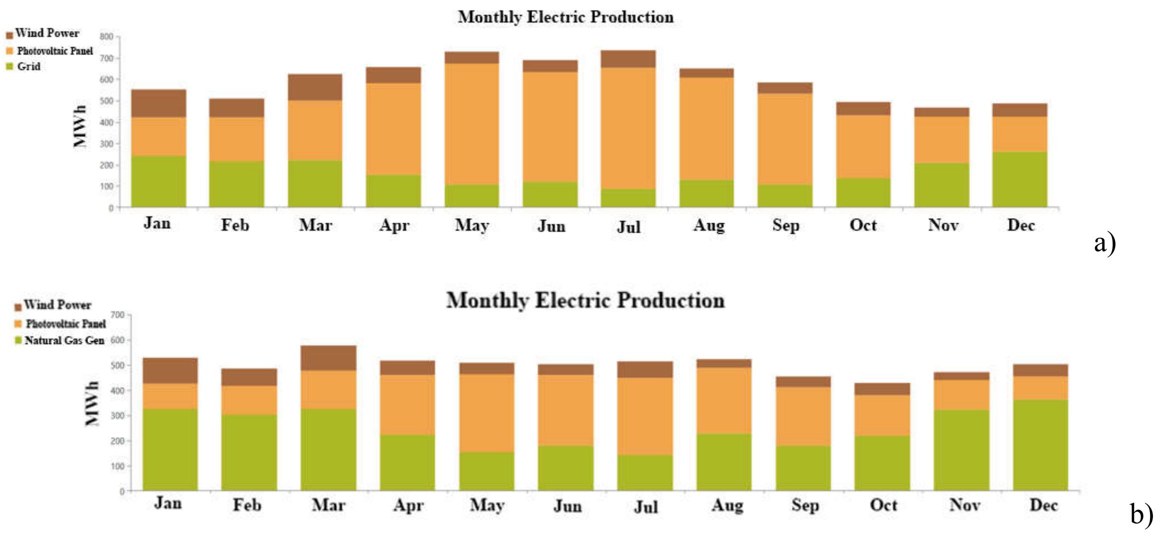

Figure 15. Electricity production distribution a) on-grid b) off-grid

Figure 15 (a) shows the monthly electricity generation distribution of system components for Scenario 1. It was observed that 60.1% of the total annual electricity generation was provided by PVPs, 12.1% by wind turbines, and 27.8% by electricity purchased from the grid. Annually, PVPs generated 4,314,326 kWh of energy, while wind turbines produced 864,659 kWh. Additionally, 1,993,654 kWh of electricity was purchased from the grid over the year.

Figure 15 (b) shows the monthly electricity generation distribution of system components for off-grid Scenario 1. It was observed that 39.2% of the total annual electricity generation was provided by PVPs, 11.4% by wind turbines, and 49.4% by natural gas generators. As shown in the graph, during the summer months, a significant portion of the electricity demand is met by the PVPs s. Annually, the PVPs generate 2,353,853 kWh, the wind turbine generates 687,293 kWh, and the natural gas generator produces a total of 2,476,369 kWh.

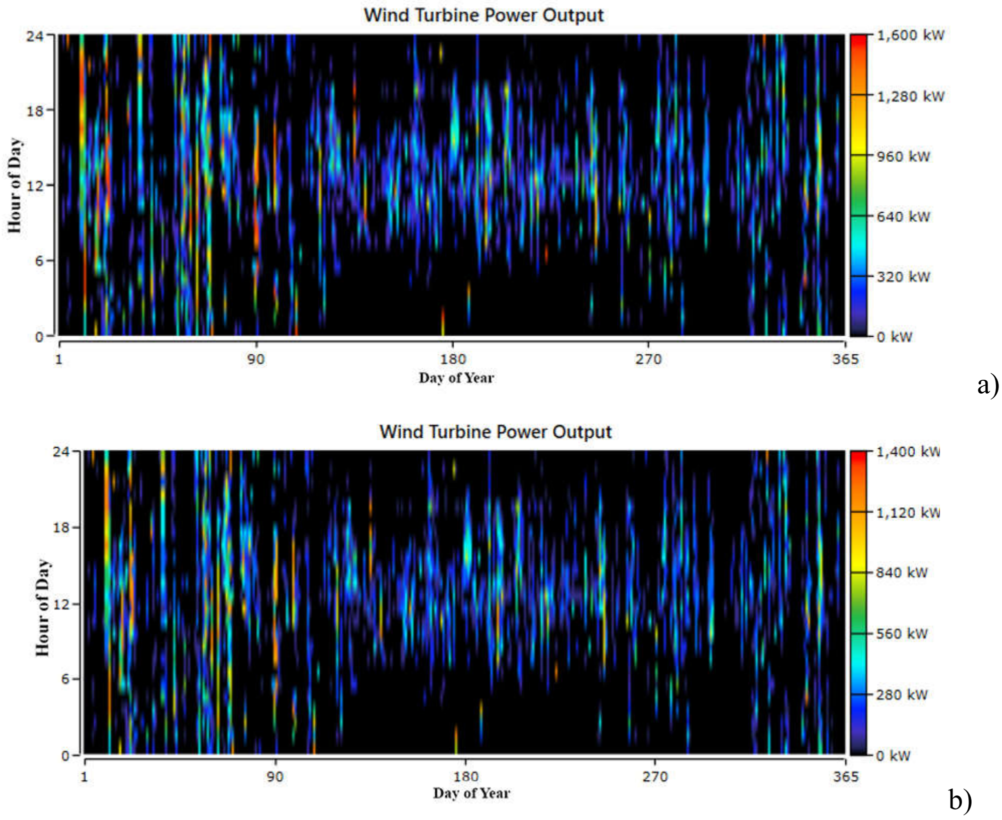

Figure 16. Wind turbine output power a) on-grid and b) off-grid

Figure 16(a), the output power of the wind turbine used in the grid-connected Scenario 1 is shown for different days and hours throughout the year. The variation in the values observed in the graph is related to wind speed and the electricity generation needs of the system. The wind turbine operates for a total of 2,901 hours annually and generates 864,659 kWh of electricity annually. The unit cost of electricity produced by wind turbines is \$0.272/kWh.

In Figure 16(b), the output power of the wind turbine used in Scenario 1 is displayed for different days and hours throughout the year. The variation in the values is influenced by both the wind speed and the system's electricity generation needs. The wind turbine operates for a total of 2,901 hours annually and generates 687,293 kWh of electricity annually. The unit cost of electricity produced by wind turbines is \$0.272/kWh.

a)

b)

Figure 17. Electrolyzer annual energy consumption a) on-grid and b) off-grid

Figure 17(a) shows the annual energy consumption of the electrolyzer in grid-connected Scenario 1. The electrolyzer integrated into the hybrid energy system produced 3,956 kg of hydrogen over the course of the year. The peak hydrogen production occurred in May, during which the electrolyzer consumed approximately 18 kW of energy. The seasonal variation in hydrogen production corresponds to the availability of excess renewable energy, particularly during periods of higher solar generation, thus reducing reliance on grid power for hydrogen production. Figure 17(b) shows the annual energy consumption of the electrolyzer in off-grid Scenario 1. In this scenario, the electrolyzer produces 4,105 kg of hydrogen annually, peaking in April and May. During these months, the electrolyzer consumed an average of 18 kW of energy. The increase in hydrogen production during these months is directly linked to the surplus of renewable energy generated by solar and wind resources, which optimizes the electrolyzer's operation under off-grid conditions. The efficiency of the system in utilizing available renewable energy to drive hydrogen production highlights the effectiveness of the off-grid configuration in maintaining continuous hydrogen generation without grid dependency.

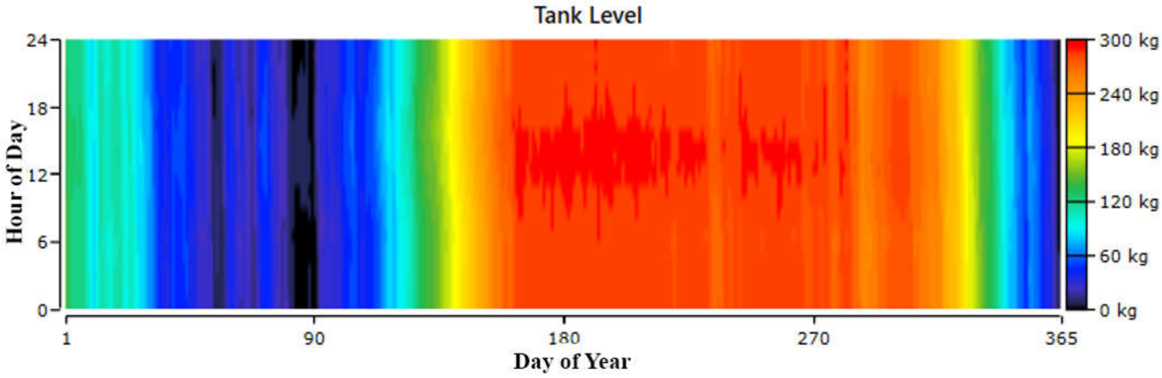

Figure 18. Hydrogen tank filling rate

Figure 18 illustrates the hydrogen tank fill levels for grid-connected (on-grid) Scenario 1 and off-grid Scenario 1 over different days and hours of the year. According to the graph, the hydrogen tank's fill level approached 100% between days 150 and 300 of the year. At full capacity, the hydrogen tank has an energy potential equivalent to 10,000 kWh. This indicates that during this period, the system produces excess renewable energy, which is efficiently stored as hydrogen for future use. Variations in the tank's fill levels correspond to fluctuations in renewable energy generation, highlighting the system's ability to balance energy production and storage.

Table 3 provides key data regarding the hydrogen storage system, including the tank's capacity to store 300 kg of hydrogen, which corresponds to 10 kWh of energy storage. The system's autonomy was calculated to be 21 hours, indicating the duration for which the stored hydrogen could supply energy without requiring additional input.

Table 3. Hydrogen storage data

Data	Value	Unit
Hydrogen Storage Capacity	300	kg
Energy Storage Capacity	10	kWh
Tank Autonomy	21.0	hr

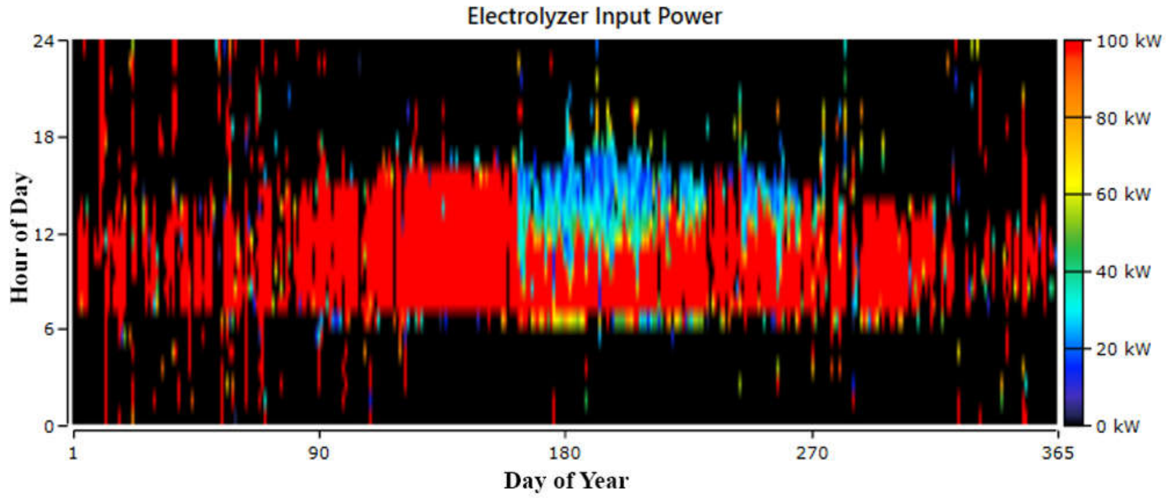

a)

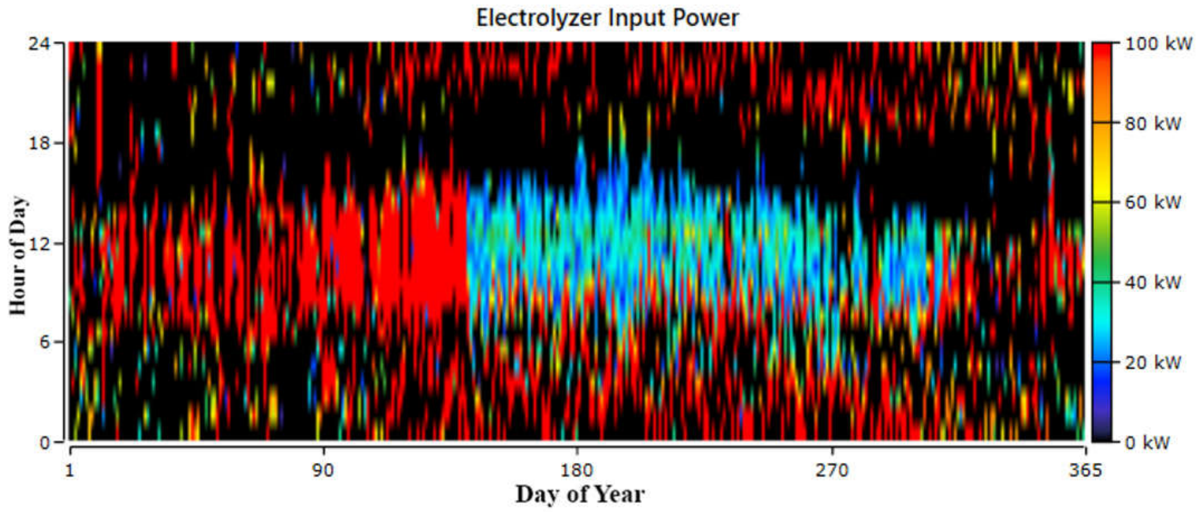

b)

Figure 19. Electrolyzer input power a) on-grid and b) off-grid

In Figure 19(a), Scenario 1 shows the power input profile of the electrolyzer, which operated for 3,127 hours annually and consumed 231,190 kWh of energy. The capacity factor of the electrolyzer was 26.4%, and the total hydrogen production reached 3,956 kg per year. These results highlight the moderate utilization of the electrolyzer within the system, which is driven primarily by surplus renewable energy generation from solar and wind resources during peak periods. The grid-connected nature of the system provides additional flexibility in balancing the energy supply and demand, which contributes to consistent year-round electrolyzer operation.

In contrast, Figure 19(b) shows the power input profile of the electrolyzer in off-grid Scenario 1. In this case, the electrolyzer operated for 3,870 hours annually, consuming 239,909 kWh of energy. The electrolyzer capacity factor was slightly higher at 27.4%, with a total annual hydrogen production of 4,105 kg. The extended operation hours and increased hydrogen output indicate greater reliance on an electrolyzer for energy storage in the absence of a grid support. This reliance necessitated more frequent operation, particularly during periods of excess renewable energy generation, to ensure energy security and system autonomy. The higher capacity factor in the off-grid scenario underscores the critical role of electrolyzers in maintaining energy balance and supporting long-term sustainability in isolated system configurations.

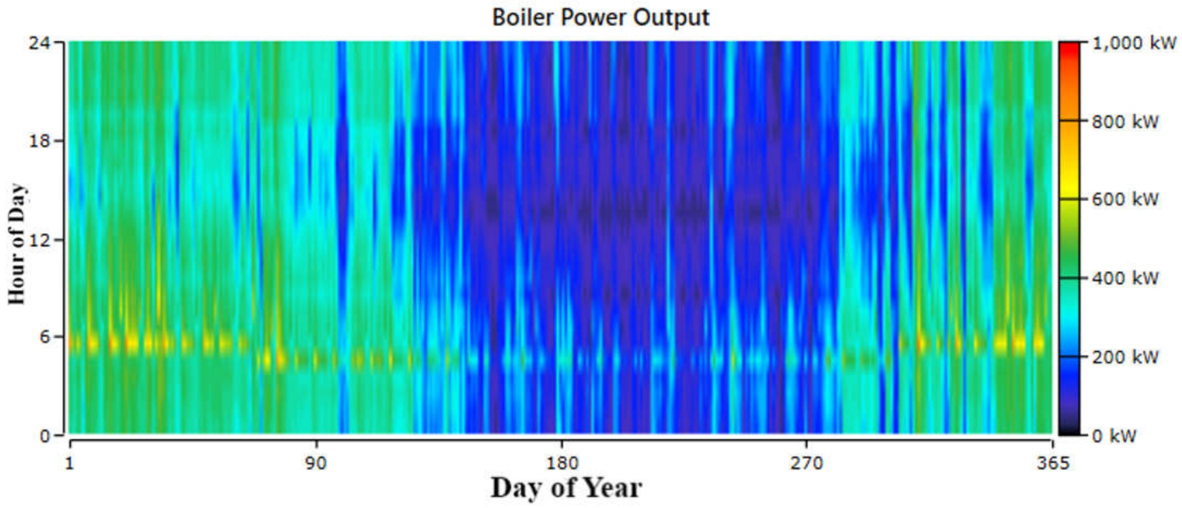

Figure 20. Thermal boiler output power

Figure 20 illustrates the boiler power outputs of both grid-connected Scenario 1 and the off-grid Scenario 1. The boiler was operated continuously for 8,760 hours throughout the year, generating a total of 2,503,479 kWh of thermal energy. The thermal efficiency of the system is 85%. As depicted in the figure, the boiler's output during summer ranges from 0 to 200 kW. The reduced output is attributed to the smaller temperature differentials during the warmer months, which result in lower heating demands. The consistent operation of the boiler throughout the year highlights its importance in meeting the system's thermal load, particularly during colder periods when the demand for heating is significantly higher.

Table 3. Hydrogen storage data

Data	Value	Unit
Hydrogen Storage Capacity	300	kg
Energy Storage Capacity	10	kWh
Tank Autonomy	21.0	hr

Cost analysis of the best on-grid scenario

The cost analysis for the on-grid system, as presented in Table 4, provides a detailed breakdown of the financial performance of each component, including capital costs, replacement expenses, operation and maintenance (O&M) costs, fuel expenditures, and salvage values. The Autosize Generator, with a capital cost of $1,150,000.00 and substantial replacement and O&M costs of $2,609,168.97 and $2,869,971.74, respectively, accumulates a total expenditure of $10,401,569.41, driven by significant fuel consumption of $4,061,825.86. The Generic Boiler, which relies primarily on fuel, incurs a total cost of $981,813.33 without additional O&M or capital expenses. The Generic Electrolyzer had a moderate capital cost of $15,000.00 and minimal replacement and O&M costs of $7,354.08 and $15,491.17, respectively, resulting in a total cost of $35,848.03 after considering a salvage value of $1,997.22. The Grid component contributes notable savings, reflected in a negative O&M cost of -$4,818,449.27, positively affecting the system's economics. The Hydrogen Tank, with a capital cost of $130,000.00, incurs a total of $159,045.95 due to O&M expenses. The SunPower E20-327 solar panel system, with a capital investment of $3,285,946.49 and O&M costs of $978,906.89, brings its total cost to $4,264,853.38.

The Surrette 6 CS 25P battery, which serves as a critical storage component, incurs a total cost of $4,051,048.49 due to high replacement costs of $3,225,203.48 and O&M expenses of $239,725.87. The System Converter, with a capital cost of $467,224.88 and a replacement cost of $343,600.86, contributes $717,510.65 to the system's total cost after factoring in a salvage value of $93,315.08. Collectively, the system's financial evaluation reveals capital costs of $5,048,171.37, replacement costs of $2,960,123.90, and

O&M costs of -$925,033.53. The inclusion of fuel costs ($5,043,644.19) and salvage values (-$384,709.46) results in a comprehensive total system cost of $11,742,196.47. This cost analysis underscores the critical role of capital investments, operational expenditures, and lifecycle costs in determining the economic feasibility of on-grid energy systems, offering essential insights for long-term financial planning and investment decisions in renewable energy infrastructure.

Table 4. Cost table of on-grid system

Component	Cost ($)	Replacement ($)	O&M ($)	Fuel ($)	Salvage ($)	Total ($)
Autosize Genset	1,150,000.00	2,609,168.97	2,869,971.74	4,061,825.86	289,397.16	10,401,569.41
Generic Boiler	0.00	0.00	0.00	981,818.33	0.00	981,818.33
Generic Electrolyzer	15,000.00	7,354.08	15,491.17	0.00	1,997.22	35,848.03
Grid	0.00	0.00	4,818,449.2	0.00	0.00	4,818,449.27
Hydrogen Tank	130,000.00	0.00	29,045.95	0.00	0.00	159,045.95
SunPower E20-327	3,285,946.49	0.00	978,906.89	0.00	0.00	4,264,853.38
System Converter	467,224.88	343,600.86	0.00	0.00	93,315.08	717,510.65
System	5,048,171.37	2,960,123.90	925,033.53	5,043,644.19	384,709.46	11,742,196.47

Table 5. Cost table of the off-grid system

Component	Cost ($)	Replacement($)	O&M($)	Fuel($)	Salvage($)	Total($)
Autosize Genset	1,150,000.00	5,188,582.11	4,864,789.16	2,800,745.78	641,956.39	13,362,160.65
Eocycle EO20	1,150,000.00	534,359.56	22,268.56	0.00	361,746.45	1,344,881.67
Generic Boiler	0.00	0.00	0.00	981,818.33	0.00	981,818.33
Generic Electrolyzer	15,000.00	7,354.08	15,491.17	0.00	1,997.22	35,848.03
Hydrogen Tank	130,000.00	0.00	29,045.95	0.00	0.00	159,045.95
SunPower E20-327	3,526,547.68	0.00	1,050,583.70	0.00	0.00	4,577,131.38
Surrette 6 CS 25P	680,900.00	3,325,203.48	239,725.87	0.00	194,780.86	4,051,048.49
System Converter	567,644.83	417,450.48	0.00	0.00	113,371.15	871,724.17
System	7,220,092.52	9,472,949.71	6,221,904.39	3,782,564.11	1,313,852.07	25,383,658.66

Based on the off-grid system cost table in Table 5, the cost analysis provides a comprehensive breakdown of the financial performance, covering capital costs, replacement expenses, operation and maintenance (O&M) costs, fuel expenditures, salvage values, and total system costs. The Autosize Generator, with a capital cost of $1,150,000.00, replacement cost of $5,188,582.11, and O&M cost of $4,864,789.16, leads to a total expenditure of $13,362,160.65, largely due to substantial fuel consumption costing $2,800,745.78. The Eocycle EO20 wind turbine, despite an initial capital cost of $1,150,000.00, achieves a lower total cost of $1,344,881.67 due to the absence of fuel costs and a salvage value of $361,746.45. The Generic Boiler, primarily relying on fuel, incurs a total cost of $981,813.33 without additional capital or O&M expenses. The Generic Electrolyzer, with a capital cost of $15,000.00, minimal replacement costs of $7,354.08, and O&M expenses of $15,491.17, results in a total cost of $35,848.03. The Hydrogen Tank adds $159,045.95 to the system's cost. The SunPower E20-327 solar panel system, with a replacement cost of $1,050,583.70 and no fuel expense, totals $4,577,131.38. The Surrette 6 CS 25P battery, a crucial storage component, incurs a total cost of $4,051,048.49 due to high replacement costs of $3,325,203.43 and O&M costs of $239,725.87. The System Converter, with a capital cost of $567,644.83 and replacement cost of $417,450.48, adds up to $871,724.17 to the system's total cost.

In summary, the system's financial evaluation reveals total capital costs of $7,220,092.52, replacement costs of $9,472,949.71, and O&M costs of $6,221,904.39. Including fuel costs ($3,782,564.11) and subtracting salvage values (-$1,313,852.07), the comprehensive total cost amounts to $25,383,658.66. This cost analysis highlights the importance of capital and operational expenditures in assessing the economic sustainability of off-grid energy systems, offering essential insights for long-term financial planning and investment in renewable energy infrastructure.

Cost-Effective Energy System Scenario

Figure 21 illustrates the lowest-cost scenario in which the system integrates various energy sources and storage methods to meet both electrical and thermal demands. The primary components include a natural gas generator, a grid connection, wind energy, and PVPs. These components were designed to handle a daily electrical load of 11,103.87 kWh and a peak demand of 1,501.00 kW. The system also supports an EV charging station, which requires 300.00 kWh per day and has a peak demand of 600.00 kW. Excess energy generated from renewable sources is stored in batteries to ensure continuous energy availability. Additionally, an electrolyzer converts surplus electricity into hydrogen, which is stored in a hydrogen tank for later use or supplied directly to the hydrogen tank. For thermal demands, a boiler was utilized, consuming 6,858.85 kWh per day, with a peak consumption of 889.89 kW. The integration of these components through an AC/DC converter ensures balanced and efficient energy distribution, thus optimizing costs by leveraging renewable energy sources and reducing dependency on grid electricity. This system configuration successfully meets energy demands while maintaining cost-effectiveness and sustainability.

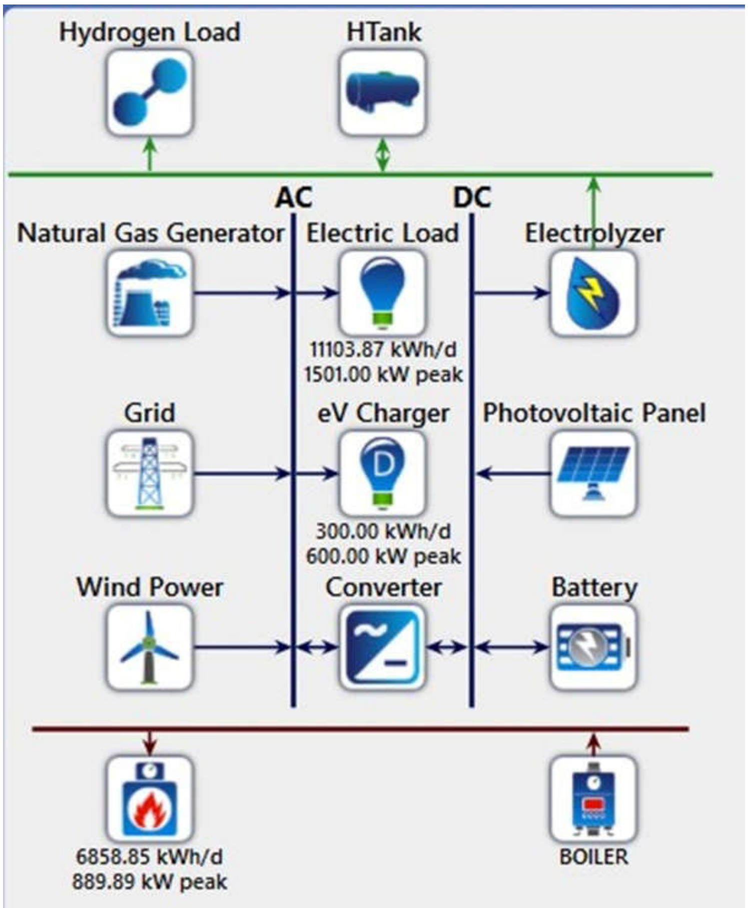

Figure 21. Thermal boiler output power

Sensitivity Analysis: Impact of Fuel Type on the System

In the sensitivity analysis conducted within the simulation, the effects of natural gas, gasoline, and diesel fuel types on the system were examined, assuming that the prices of these fuels may increase over time. It is projected that the unit price of natural gas could reach $0.143, $0.17, and $0.20. Diesel prices were anticipated to rise to $1.34, $1.50, and $1.75 per liter, whereas gasoline prices were expected to increase to $1.38, $1.45, and $1.65 per liter. This analysis provides a detailed understanding of how the system responds to changes in fuel costs, thereby helping to evaluate the system's long-term viability and resilience against market fluctuations.

Currently, natural gas is considered one of the most environmentally friendly fossil fuel options. It offers a cleaner alternative for energy production due to its low-carbon emissions and is widely used in many energy systems. However, price volatility and supply security issues are critical factors that must be carefully considered in long-term planning. Increases in natural gas prices could elevate energy costs, challenging the system's economic stability.

Diesel fuel is widely used, especially in the heavy industry and transportation sectors, because of its high energy density and broad availability. However, it is known for producing significant carbon emissions. Rising diesel prices could increase operational transportation and logistics costs, prompting energy systems to explore alternative solutions to reduce their diesel dependency.

Gasoline is primarily used in light vehicles and personal transportation. Rising gasoline prices directly affect consumers' energy costs. Higher gasoline prices may encourage a shift toward more environmentally friendly alternatives, such as electric and hybrid vehicles. Moreover, increasing gasoline costs could accelerate the transition away from gasoline use in energy systems and promote the adoption of renewable energy sources.

The price fluctuations among these three fuel types are critical variables to consider in the strategic planning of energy systems. Increased fuel costs directly affect energy production costs and may drive a faster transition to renewable energy sources. Furthermore, considering the emission profiles and environmental impacts of different fuel types is essential for developing sustainable and economically efficient energy solutions. Ultimately, analyzing price changes in natural gas, diesel, and gasoline is crucial for understanding the dynamic nature of energy systems and shaping long-term sustainability strategies .

Effect of Varying Natural Gas Prices on the System

In the sensitivity analysis conducted as part of the simulation, the potential increase in natural gas prices over time was considered, with projections suggesting that prices could rise to $0.143, $0.17, and $0.20 per cubic meter. Similarly, diesel prices are projected to increase to $1.34, $1.50, and $1.75 per liter. This approach allowed for a detailed examination of how the system responds to changes in fuel costs, providing valuable insights into its long-term sustainability and resilience against market fluctuations.

Figure 22(a) presents the impact of rising natural gas prices on the electricity generation and fuel costs of the best on-grid scenario. As natural gas prices increase from $\$0.14/m^3$ to $\$0.20/m^3$, the annual energy output of the natural gas generator decreases from approximately 2 x 10^7 kWh to around 1 x 10^7 kWh. This demonstrates that higher natural gas costs make generator operation less economically viable, leading the energy generation system to shift toward more cost-effective alternatives. While rising natural gas prices lead to higher fuel costs, a reduction in generator use causes total fuel costs to drop from an initial value of approximately $800,000 to approximately $300,000. This decline suggests a shift toward a more economical energy consumption preference toward grid electricity.

Figure 22(b) shows the effect of natural gas price on the generator for the best off-grid scenario. Unlike the on-grid scenario, there is no significant change in the annual energy output of natural gas generators as prices increase from $\$0.14/m^3$ to $\$0.20/m^3$. The generator's energy production remained steady at approximately 2,970,246 kWh per year, indicating that the generator's output was maintained regardless of fuel price fluctuations. However, fuel costs rise as natural gas prices rise. Initially, fuel costs are approximately $100,000, but they rise to nearly $200,000 when natural gas prices reach $\$0.20/m^3$, showing that higher fuel prices directly impact operational costs without affecting the generator's output.

These results clearly demonstrate how rising natural gas prices affect generator utilization in both on-grid and off-grid systems. Although higher costs reduce generator use and fuel expenses in on-grid systems, off-grid systems maintain stable generator output, but fuel costs rise significantly with price fluctuations.

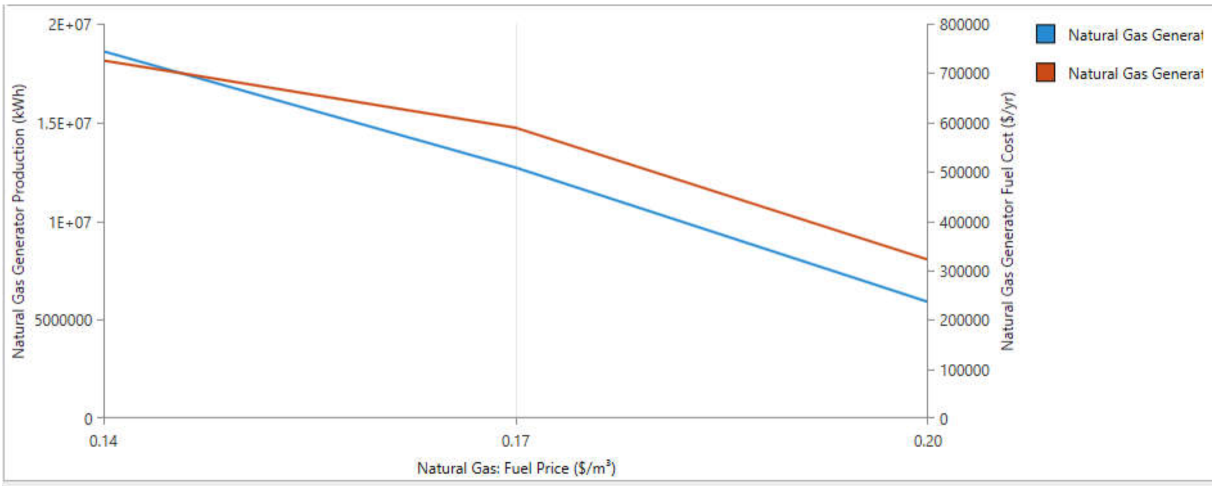

a)

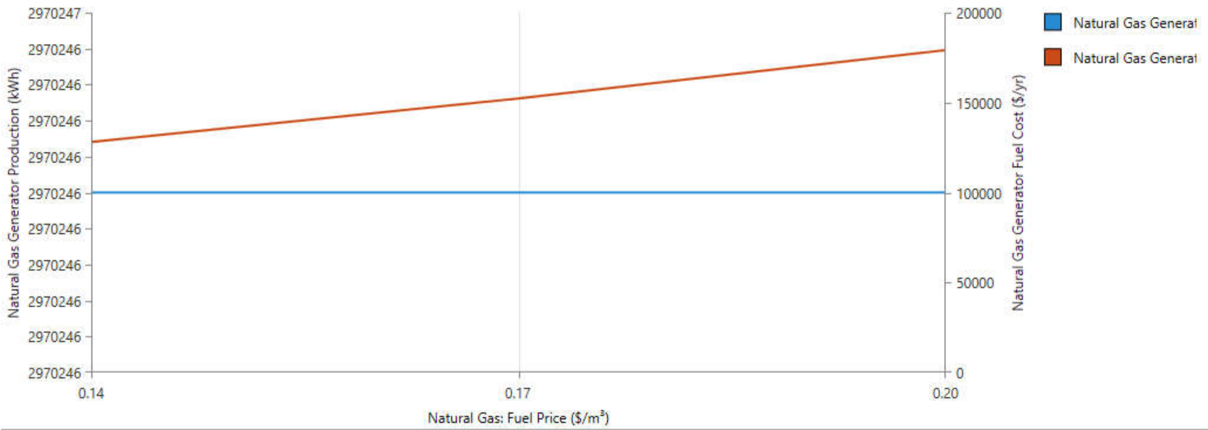

b)

Figure 22. Effect of natural gas price a) on-grid and b) off-grid

Impact of Electrolyzer Efficiency on the System

The electrolyzer efficiency plays a critical role in the performance of energy systems, as demonstrated by the Homer scenarios. High-efficiency electrolyzers are capable of producing the same amount of hydrogen with less energy input, thereby reducing overall energy costs and improving the system efficiency. Conversely, low-efficiency electrolyzers consume more energy, leading to higher costs and less effective utilization of renewable electricity. Analyzing the effects of variations in electrolyzer efficiency is essential for understanding their impact on energy production costs, carbon emissions, and energy storage strategies. For instance, in scenarios where high-efficiency electrolyzers are employed, excess renewable energy can be more efficiently utilized for hydrogen production, thereby facilitating energy storage and better managing the energy surplus. Additionally, as the electrolyzer efficiency increases, the economic sustainability of renewable energy systems improves, thus reducing the reliance on fossil fuels. This shift not only enhances environmental sustainability and fortifies energy systems against long-term market fluctuations.

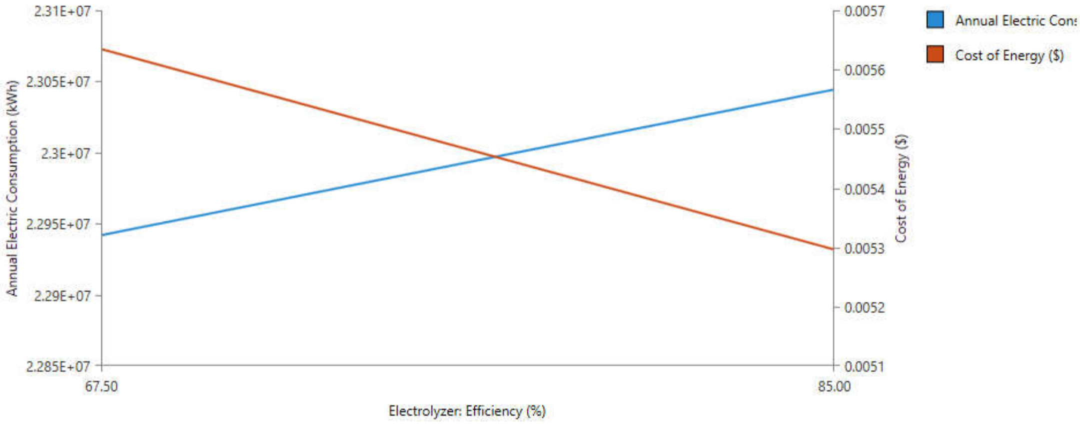

Figure 23. Effect of electrolyzer efficiency on electricity consumption and energy cost.

Impact of Average Daily Electricity Consumption of Electric Vehicle Charging Stations on the System

The average daily electricity consumption of EV charging stations is a complex topic influenced by several factors, each of which must be examined in detail to understand their effects on consumption. The first major determinant is the type of charging station. Fast-charging stations, which deliver higher power, can charge vehicles in a shorter time, resulting in daily consumption ranging from 100 to 500 kWh. In contrast, slow charging stations operate at lower power and typically consume between 10 and 50 kWh daily. Second, the frequency of use is a critical factor. High-traffic charging stations, where more vehicles are charged daily, naturally exhibit higher electricity consumption, whereas stations with less frequent use consume less electricity. The battery capacity of the vehicles also plays a significant role; vehicles with larger battery capacities require more electricity, whereas those with smaller batteries consume less. Regional grid characteristics can also influence consumption. In areas with lower electricity prices, more frequent charging may occur, whereas higher electricity prices can deter consumption. Furthermore, seasonal variations may affect usage patterns; during winter, cold weather can increase the charging time and consequently increase the electricity consumption, whereas hot weather in summer can have a similar but variable impact on the charging duration. The interplay of these factors means that the average daily electricity consumption of EV charging stations can vary widely, ranging from 10 to 500 kWh. This broad range highlights the importance of understanding and managing the energy demand of charging stations, particularly as EV adoption continues to grow. Effective energy management and planning for EV charging infrastructure is essential for optimizing the performance of energy systems and ensuring their sustainability, especially in light of the increasing integration of renewable energy sources.

Figure 24 (a) presents the relationship between the average daily energy consumption of EV charging stations and the total NPC and energy cost of an off-grid system. The analysis shows that the scaled average daily energy consumption of the EV charging stations varies between 250 and 300 kWh. This detailed examination revealed the influence of EV charging station consumption on system costs. According to the data, when the daily energy consumption of the EV charging stations is 250 kWh, the total NPC is approximately \$2.48 x 10^7. As consumption increases, the total cost also rises, peaking at 280 kWh, which is approximately \$2.56 x 10^7. However, once daily consumption exceeds 280 kWh, the total cost begins to decrease, reaching around \$2.52 x 10^7 at 300 kWh. Similarly, energy costs exhibit a comparable trend. For 250 kWh of daily energy consumption, the energy cost is approximately \$0.304/kWh. As consumption increases, energy costs rise, peaking at 280 kWh at approximately \$0.31/kWh. Beyond 280 kWh, energy costs decrease, returning to approximately \$0.304/kWh at 300 kWh.

In Figure 24(b), an analysis of the on-grid system shows that when the daily energy consumption of the EV charging stations is 250 kWh, the total NPC is approximately \$3,010,000. As consumption increases, the total cost rises, reaching approximately \$3,240,000 at 280 kWh and continuing to climb to approximately \$3,300,000 at 300 kWh. The energy cost is approximately \$0.0044/kWh for 250 kWh of daily consumption. As consumption increases, energy costs rise, peaking at 280 kWh at approximately \$0.0052/kWh and further increasing to approximately \$0.0056/kWh at 300 kWh. The analysis of these graphs reveals that the daily energy consumption of EV charging stations initially increases costs up to a certain threshold, after which costs begin to decline. This trend suggests that there is an optimal usage level for charging stations. Specifically, the data indicate that the maximum impact on costs occurs at 280 kWh, and costs decrease beyond this point. These findings are critical for developing strategies aimed at optimizing energy consumption and minimizing costs. They highlight the importance of identifying the optimal consumption threshold for EV charging stations to enhance both cost and energy efficiency.

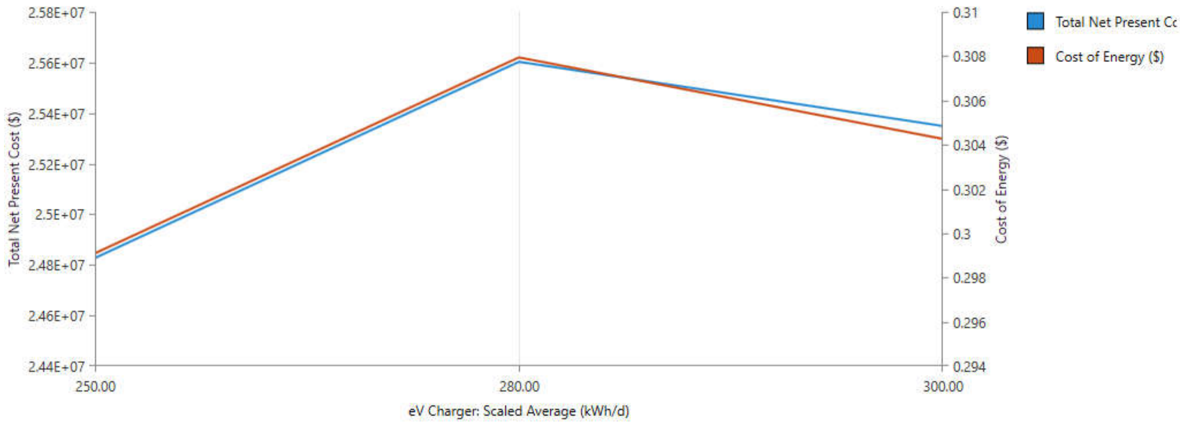

a)

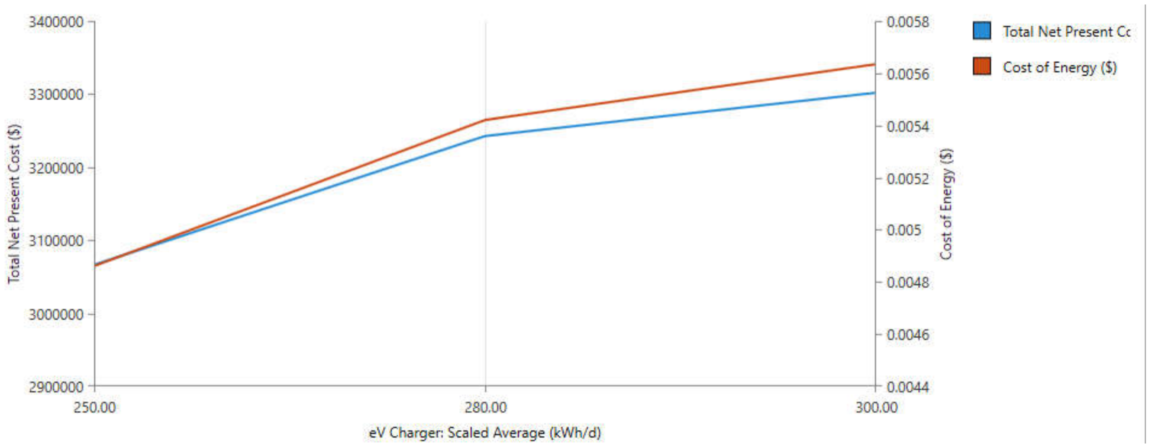

b)

Figure 24. EV charging effect on daily electricity consumption off-grid b) on-grid

Impact of Minimum Load Ratio on Electric Vehicle Charging Station System

The minimum load ratio of EV charging stations represents the lowest energy demand required for stations to operate efficiently and safely. This ratio is crucial for optimizing energy consumption and preventing energy waste (Singh, et al., 2024). If charging stations fail to meet the minimum load requirement, device efficiency may decrease, potentially causing unexpected energy fluctuations. Therefore, considering minimum load ratios in the design and operation of charging infrastructure plays a critical role in enhancing the effectiveness of energy management. Accurately determining these minimum load ratios helps reduce energy costs while ensuring reliable and long-term operation of charging stations (Silapan et al., 2024).

Figure 25 (a) shows the analysis of an off-grid system, examining the effect of the minimum load ratio of EV charging stations on the total NPC and energy cost. The minimum load ratio of the stations varies between 20% and 80%, which significantly affects the cost.

According to the data, when the minimum load ratio is 20%, the total NPC is approximately \$2.48 x 10^7. As the ratio increases to 50%, the total cost peaks at approximately \$2.54 x 10^7. However, when the minimum load ratio reaches 80%, the total cost decreases to approximately \$2.46 x 10^7. This trend indicates that the load ratio initially leads to cost increases; however, after surpassing a certain level, further increases in the ratio result in lower costs. In terms of energy costs, when the minimum load ratio is 20%, the cost is approximately $0.304/kWh. As the load ratio increases to 50%, energy costs rise to approximately $0.308 per KWh. However, at an 80% load ratio, the energy cost decreases to approximately $0.296/kWh. This demonstrates a similar trend, where costs increase up to a certain point and then begin to decrease as the load ratio exceeds the optimal threshold. Figure 25 (b) presents the analysis of an on-grid system. When the minimum load ratio is 20%, the total NPC is approximately $3,335,000. As the ratio increases to 50%, the total cost decreases to approximately $3,190,000. However, when the load ratio reaches 80%, the total cost rises again to approximately $3,230,000. This indicates that the minimum load ratio is optimal at a specific level, and costs increase when the ratio is below or above this level. The energy cost is approximately $0.0057/kWh at a minimum load ratio of 20%, the cost is approximately $0.0057/kWh. As the ratio increases to 50%, the cost decreases to approximately $0.0050/kWh but rises again to approximately $0.0053/kWh at an 80% load ratio. This suggests that energy costs fluctuate based on the minimum load ratio and increase after a specific threshold.

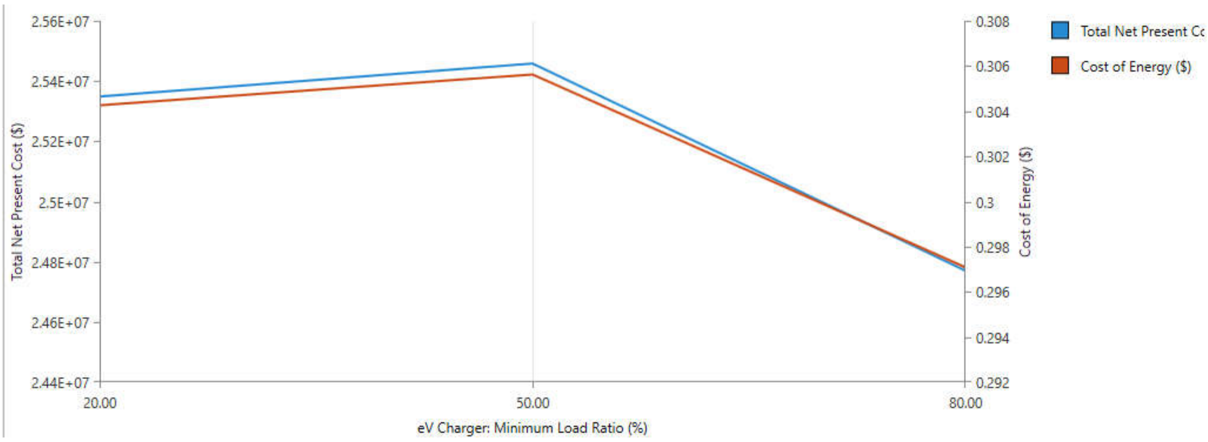

a)

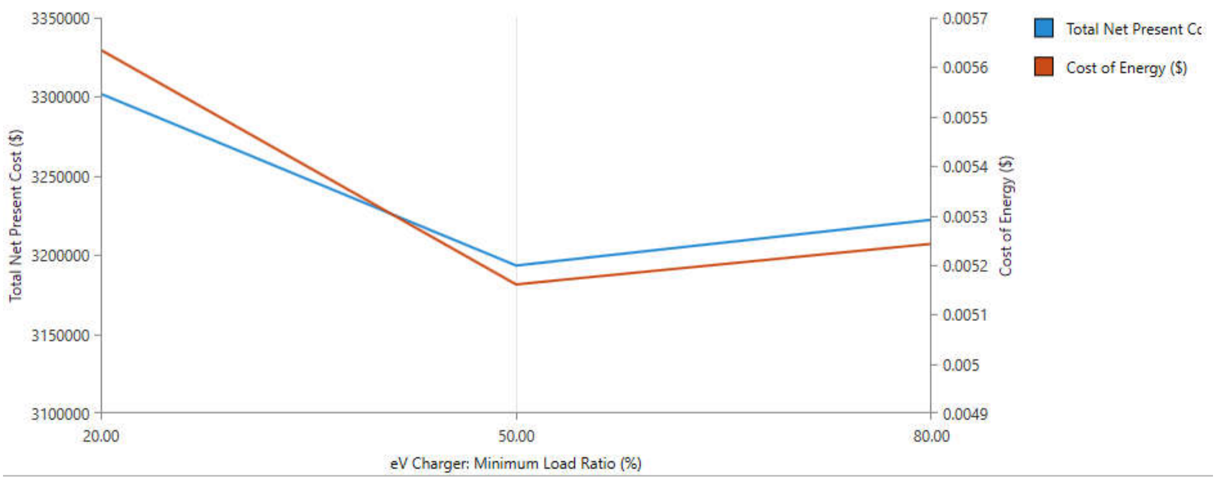

b)

Figure 25. Effect of minimum load ratio on eV charging a) off-grid b) on-grid

These findings demonstrate that the minimum load ratio of EV charging stations is a critical parameter for cost optimization in both off-grid and on-grid systems. There is an optimal load ratio at which charging stations operate most efficiently and economically, and deviations from this ratio lead to significant changes in costs. Therefore, careful consideration of such parameters is essential for achieving cost-effectiveness and operational efficiency.

Environmental Assessment

In addition to the cost results, the emission values of the scenarios play a critical role in minimizing environmental impacts. Table 6 presents the emission values for the best on-grid and off-grid scenarios. These values highlight the environmental footprint of each system and demonstrate the relative environmental performance of on-grid and off-grid designs.

Table 6. Emission values of the best scenarios for on-grid and off-grid

Emission	On grid	Off grid	Unit
Carbon Dioxide	1838833	2292291	kg/yr
Carbon Monoxide	0	14778	kg/yr
Unburned Hydrocarbons	0	645	kg/yr
Particulate Matter	0	89,6	kg/yr
Sulfur Dioxide	5463	0	kg/yr
Nitrogen Oxides	2671	13883	kg/yr

From the emission data, it is evident that the off-grid system, which relies more heavily on fossil fuels, generates significantly higher emissions, particularly in terms of carbon dioxide (CO_2), carbon monoxide (CO), and nitrogen oxides (NOx). In contrast, the on-grid system benefits from the availability of renewable energy sources and the grid, which reduces its reliance on polluting fuels, thereby resulting in lower overall emissions. The on-grid scenario generates 51.2% of its electricity from renewable energy sources, according to the HOMER simulation. In comparison, the off-grid scenario generates only 17.9% of its electricity from renewable sources. This substantial difference in renewable energy integration not only leads to lower emissions in the on-grid scenario but also contributes to a more sustainable operational profile. When considering carbon dioxide emissions, the on-grid system emits approximately 1.84 million kg of CO_2 annually, whereas the off-grid system produces 2.29 million kg. This 24% reduction in CO_2 emissions for the on-grid system can be attributed to its higher reliance on renewable energy sources, such as solar and wind, alongside the ability to draw energy from the grid when needed.

Furthermore, harmful pollutants such as CO, unburned hydrocarbons, particulate matter, and NOx are completely absent in the on-grid scenario or are significantly lower than in the off-grid scenario. The off-grid system, which relies on fossil fuel-based generation, contributes to higher emissions of these pollutants due to the combustion of fuels like diesel or natural gas. Sulfur dioxide (SO_2) emissions are also a notable point of comparison. While the on-grid system produces 5,463 kg/yr of SO_2 due to some grid reliance on fossil fuels, the off-grid system, which does not utilize sulfur-emitting sources, produces none. However, the reduction in NOx and other harmful gases in the on-grid system outweighs this slight increase in SO_2 emissions.

In summary, the environmental assessment clearly indicates that the on-grid scenario is more favorable from both an emissions and cost perspective. The substantial integration of renewable energy in on-grid scenarios reduces the environmental footprint, making it a more sustainable option for energy generation. As renewable energy technologies continue to advance and their costs decline, this trend is expected to grow stronger, further emphasizing the need to prioritize grid-connected systems that maximize renewable energy use. The off-grid scenario, while offering independence, incurs higher environmental costs because it relies on fossil fuels, underscoring the importance of renewable energy integration in achieving long-term sustainability goals.

Conclusion and Recommendations

This study aimed to design grid-connected and off-grid hybrid energy systems to meet the 2024 monthly consumption values of a public building located 5.5 km away from the city center using HOMER software. Various scenarios were modeled, and the optimal system configuration was determined by HOMER by comparing different results. The key components in these scenarios include PVPs, WTs, hydrogen tanks, electrolyzers, thermal boilers, natural gas generators, converters, and batteries. Differences between scenarios arise from the components used and the sensitivity analyses performed. The inclusion or exclusion of generators and grid connections, changes in system components, and variations in the sensitivity analysis parameters were critical for identifying the system that best met the energy load requirements.

From the analysis, the hybrid energy system consisting of PVPs, a grid, WTs, thermal boilers, hydrogen tanks, electrolyzers, and batteries was determined to be the optimal solution, with an NPC of $10.8 million and an LCOE of $0.0764/kWh. Additionally, this system provided 51.2% of its energy from renewable sources, making it the most suitable choice from both a cost and environmental perspective. However, if an off-grid configuration is required, the first off-grid scenario emerges as a more viable option. This system, with an NPC of $25.3 million and an LCOE of $0.304/kWh, consists of PVPs, WTs, hydrogen tanks, electrolyzers, thermal boilers, natural gas generators, and batteries.

Given current considerations such as cost, renewability, and environmental impacts, the grid-connected scenario is the most practical choice. The integration of renewable energy sources into modern energy systems is essential for sustainable development, but it requires a thorough feasibility analysis before implementation. It is crucial to first assess the solar, wind, hydrogen, and geothermal energy potential of the chosen region. Additionally, a detailed understanding of the required energy loads is vital for accurate system design.

Hybrid energy systems are highly dependent on meteorological data of the region and fluctuations in electricity demand. As a result, system configurations can significantly affect the economic performance of a system. Therefore, as demonstrated in this study, a detailed analysis is essential. The configurations analyzed here provide valuable insights into the use of renewable energy sources and offer an optimal solution for this particular case.

Recommendations:

1. Detailed Feasibility Studies: Before implementing hybrid renewable energy systems, comprehensive feasibility studies should be conducted, including an assessment of the region's renewable energy potential (solar, wind, hydrogen, geothermal) and a detailed analysis of energy consumption patterns.
2. Optimization of sustainability: The optimal balance between renewable energy integration and economic viability should be continuously evaluated. The inclusion of higher percentages of renewable energy in the energy mix should be encouraged because it supports long-term sustainability while reducing environmental impacts.
3. Flexibility in System Design: Energy systems should be designed with flexibility to accommodate technological and policy changes, such as advancements in storage technologies or shifts in energy regulations.
4. Environmental Impact Reduction: Future projects should prioritize minimizing carbon and other pollutants by maximizing renewable energy usage. A clear pathway to reduce reliance on fossil fuels should be established.
5. Economic Incentives: Governments and institutions should consider providing incentives or subsidies for the integration of renewable energy sources, especially hybrid systems, to make them more financially attractive.

In conclusion, this detailed analysis provides a clear framework for the successful design and implementation of hybrid renewable energy systems. Such studies are vital for ensuring the economic and technical efficiency of energy projects, ultimately contributing to the broader goals of sustainable development and environmental preservation.

References

Al-Sahlawi A.A.K, Ayob S.M., Tan C.W., et al (2024). Optimal Design of Grid-Connected Hybrid Renewable Energy System Considering Electric Vehicle Station Using Improved Multi-Objective Optimization: Techno-Economic Perspectives. Sustain 16:. https://doi.org/10.3390/su16062491

Belkhier Y., Oubelaid A., Shaw R.N. (2024). Hybrid power management and control of fuel cells-battery energy storage system in hybrid electric vehicle under three different modes. Energy Storage 6:1–22. https://doi.org/10.1002/est2.511

Chowdhury, S., Kumar, Y., Shrivastava, S., Patel, S. K., & Sangwai, J. S. (2023). A Review on the Recent Scientific and Commercial Progress on the Direct Air Capture Technology to Manage Atmospheric CO2 Concentrations and Future Perspectives. Energy & Fuels, 37(15), 10733–10757. doi: 10.1021/acs.energyfuels.2c03971

Diaf, S., Notton, G., Belhamel, M., Haddadi, M., & Louche, A. (2008). Design and techno-economical optimization for hybrid PV/wind system under various meteorological conditions. Applied Energy, 85(10), 968–987. doi: 10.1016/j.apenergy.2008.02.012

Falope T., Lao L., Hanak D., Huo D. (2024). Hybrid energy system integration and management for solar energy: A review. Energy Convers Manag X 21:100527. https://doi.org/10.1016/j.ecmx.2024.100527

Guven A.F. (2024a). Integrating electric vehicles into hybrid microgrids: A stochastic approach to future-ready renewable energy solutions and management. Energy 303:131968. https://doi.org/10.1016/j.energy.2024.131968

Güven A.F. & Yörükeren N. (2024). A comparative study on hybrid GA-PSO performance for stand-alone hybrid energy systems optimization. 42:1410–1438. https://doi.org/10.14744/sigma.2024.00

Güven A.F. &Yücel E. (2024). Sustainable energy integration and optimization in microgrids: enhancing efficiency with electric vehicle charging solutions. Electr Eng. https://doi.org/10.1007/s00202-024-02619-x

Güven, A. F. & Mete M. (2021). Balıkesir İli Erdek İlçesi İçin Bağımsız Hibrit Enerji Sisteminin Fizibilite Çalışması Ve Ekonomik Analizi. KONJES, c. 9, sy. 4, ss. 1063–1076, 2021, doi: 10.36306/konjes.978002.

Güven, A. F. (2017). Bahçelievler Belediye Başkanlık Binasının Enerji İhtiyacının Güneş ve Rüzgar Sistemi ile Karşılanması, Optimizasyonu ve Maliyet Analizi. Sinop Üniversitesi Fen Bilimleri Dergisi, 2(1), 24–36. Retrieved from http://dergipark.gov.tr/sinopfbd/issue/28364/255023.

Güven, A. F., & Hatipoğlu, C. (2022). Şebekeden Bağımsız Güneş/Rüzgâr/Biyogaz/Yakıt Hücresi/Batarya Tabanlı Hibrit Enerji Sisteminin Tekno-Ekonomik Analizi: Muğla Zaferler Köyü Vaka Çalışması. EMO Bilimsel Dergi, 12(1), 53-65.

Güven, A. F., & Mengi, O. Ö. (2023). Assessing metaheuristic algorithms in determining dimensions of hybrid energy systems for isolated rural environments: Exploring renewable energy systems with hydrogen storage features. Journal of Cleaner Production, 428(September). doi: 10.1016/j.jclepro.2023.139339

Güven, A. F., & Poyraz, E. (2021). Feasibility Study and Techno-Economic Analysis of Stand-Alone Hybrid Energy System for Muğla Province Köyceğiz. Karadeniz Fen Bilimleri Dergisi, 11(1), 70–85. doi: 10.31466/kfbd.880437.

Güven, A. F., & Yörükeren, N. (2022). Bir Hibrit Enerji Sisteminin Parçacık Sürüsü Optimizasyon Algoritması- Genetik Algoritma ve Gri Kurt Optimizasyon Algoritma Tekniği ile Enerji Yönetimi ve Optimizasyonu: Yalova Üniversitesi için bir vaka çalışması. Karadeniz Fen Bilimleri Dergisi, 12(2), 853–879. doi: 10.31466/kfbd.1169643

Güven, A. F., & Yücel, E. (2023). Application of HOMER in assessing and controlling renewable energy-based hybrid EV charging stations across major Turkish cities. International Journal of Energy Studies, 8(4), 747–780. doi: 10.58559/ijes.1324236.

Güven, A. F., Türkmen, Ş., Aşıklı, E., & Örnek, G. (2023). Investigating the Effects of Different Types of Battery Impacts in Energy Storage Systems on Standalone Hybrid Renewable Energy Systems. Karadeniz Fen Bilimleri Dergisi, 13(3), 943–964. doi: 10.31466/kfbd.1275823.

Güven, A.F. (2024b). Heuristic techniques and evolutionary algorithms in microgrid optimization problems, in: Microgrid, CRC Press.

Hasanien H.M., Alsaleh I., Tostado-Véliz M., et al (2024). Hybrid particle swarm and sea horse optimization algorithm-based optimal reactive power dispatch of power systems comprising electric vehicles. Energy 286:. https://doi.org/10.1016/j.energy.2023.129583

Jui J.J., Ahmad M.A., Molla M.M.I., Rashid M.I.M. (2024). Optimal energy management strategies for hybrid electric vehicles: A recent survey of machine learning approaches. J Eng Res 12:454–467. https://doi.org/10.1016/j.jer.2024.01.016

Nandi, S., Ghatak, S. R., Sannigrahi, S., & Acharjee, P. (2024). Coordinated planning and operation of PV-hydrogen integrated distribution network incorporating daily-seasonal green hydrogen storage and EV charging station. *International Journal of Hydrogen Energy*, *90*(August), 134–158. doi: 10.1016/j.ijhydene.2024.09.402

Okafor, C. E., & Folly, K. A. (2024). Optimal Sizing of Battery Energy Storage System (BESS) for Multiple Applications using Regression Analysis and Deep Sleep Optimizer Algorithm . 1 . Introduction Many researchers around the world have noted the crucial needs of battery energy storage sys. *Scientific African*, e02424. doi: 10.1016/j.sciaf.2024.e02424

Sadeghi, A., Maleki, A., & Haghighat, S. (2024). Techno-Economic Analysis and Optimization of a Hybrid Solar-Wind- Biomass-Battery Framework for the Electrification of a Remote Area : A. *Energy Conversion and Management: X*, 100732. doi: 10.1016/j.ecmx.2024.100732

Silapan, S., Patchanee, S., Kaewdornhan, N., Somchit, S., & Chatthaworn, R. (2024). Optimal Sizing and Locations of Fast Charging Stations for Electric Vehicles Considering Power System Constraints. *IEEE Access*, *12*(September). doi: 10.1109/ACCESS.2024.3466969

Singh, A., Kumar, A., K.A., C., & Maulik, A. (2024). DC microgrid operation with hybrid energy storage considering islanding constraints and demand response coordination: A bi-level Stackelberg game approach. *Journal of Energy Storage*, *102*(PA), 113913. doi: 10.1016/j.est.2024.113913